electronics

MDPI

Article

Multi-UAV Enabled Data Collection with Efficient Joint Adaptive Interference Management and Trajectory Design

Weichao Pi and Jianming Zhou *

School of Electronic and Information, Beijing Institute of Technology, Beijing 100081, China; peao_kelvin@bit.edu.cn

* Correspondence: zhoujm@bit.edu.cn

Abstract: This paper studies interference in a data collection scenario in which multiple unmanned aerial vehicles (UAVs) are dispatched to wirelessly collect data from a set of distributed sensors. To improve the communication throughput and minimize the completion time, we design a joint resource allocation and trajectory optimization framework that not only is compatible with the traditional time-division scheme and interference coordination scheme but also combines their advantages. First, we analyse a basic quasi-stationary scenario with two UAVs and four devices, in which the two UAVs hover at optimal displacements to execute the data collection mission, and it is proven that the proposed optimal resource allocation and trajectory solution is adaptively adjustable according to the severity of the interference and that the common throughput of the network is non-decreasing. Second, for the general mobile case, we design an efficient algorithm to jointly address resource allocation and trajectory optimization, in which we first apply the block coordinate descent method to decompose the original non-convex problem into three non-convex sub-problems and then employ a dedicated genetic algorithm, a penalty function and the sequential convex approximation (SCA) technique to efficiently solve the individual sub-problems and obtain a satisfactory locally optimal solution with an adaptive initialization scheme. Subsequently, numerical experiments are presented to demonstrate that the completion time of the data collection task with our proposed method is at least 25% shorter than those with several baseline dynamic orthogonal schemes when 4 UAVs are deployed. Finally, we provide a practical application principle concerning the maximum suitable number of UAVs to avoid the inherent deficiencies of the proposed algorithm.

Keywords: multiple UAV; data collection; joint resource and trajectory design; interference management

Citation: Pi, W.; Zhou, J. Multi-UAV Enabled Data Collection with Efficient Joint Adaptive Interference Management and Trajectory Design. *Electronics* **2021**, *10*, 547. https://doi.org/10.3390/electronics10050547

Academic Editor: Sang-Woon Jeon

Received: 13 January 2021
Accepted: 22 February 2021
Published: 26 February 2021

1. Introduction

With rapid advances in technology for unmanned aerial vehicles (UAVs), also known as drones, increasingly effective applications of UAVs are emerging in a variety of scenarios, such as area surveillance and inspection [1], environmental monitoring [2,3], remote sensing [4], packet delivery [5], intelligent agriculture [6] and wireless communication [7–9]. Specifically, with the upcoming era of 5th-generation communication, the enormous surge in demand for high throughput, low latency and flexible and fast deployment for new communication networks is expected to accelerate the deployment of flying drones with different altitudes in practical scenarios to support existing wireless networks [10], as an alternative way to satisfy stringent quality of service (QoS) demands because of their advantages of flexible deployment, full controllability, broad potential coverage and continuous cost reduction, although many open challenges remain unsolved [11,12].

By virtue of unceasing academic efforts and explorations, the advantages of deploying UAVs for communication are gradually being specified. In general, UAVs in the sky have a higher possibility of line-of-sight (LoS) links than traditional terrestrial communication links, which are degraded by shadowing and large- and small-scale fading. Thus, the QoS of future networks could be significantly enhanced through the deployment of UAVs

because of their ability to establish better channel links. In addition, the agility, mobility and flexibility of a UAV allow it to hover at close distances and even at low vertical altitudes to improve the spectral efficiency of a network [13]. Based on the above merits of drones, there has been sustained and growing interest from both the industrial and academic communities in an efficient framework for network enhancement assisted by the deployment of UAVs. Correspondingly, several pioneering Internet and communication companies and government agencies have proposed related projects, such as the Loon project in the stratosphere developed by Google [14], the "Drones and networks: Ensuring safe and secure operations" white paper released by Ericsson [15], a UAV-based project conceived and conducted by Facebook [16], a drone-based mobile solution operated by EE for rural mobile coverage and disaster recovery [17] and a cellular-connected planning project conducted by AT&T [18].

Specifically, the benefits offered by the high mobility of UAVs are attracting much attention in the emerging context of Internet of Things (IoT) applications, for which the cost of traditional terrestrial network coverage is unaffordable and even infeasible in most cases [19–22]. By contrast, UAVs can be dispatched as data collectors or receivers to wirelessly harvest data uploaded by various sensors distributed over a remote area in an energy-saving way, hence remedying the insufficiencies of the present cellular networks.

However, despite the above advantages, the high mobility and flexible deployment of UAVs also yield many theoretical challenges. In particular, the development of guidelines for designing a spectrally efficient UAV-enabled network by exploiting the resources and trajectories of the UAVs involves complicated resource allocation and flight strategies, and thus, any corresponding optimization framework leads to highly non-linear or non-convex problems, which are difficult to address in general. Nevertheless, the upcoming IoT era and the requirements of next-generation communication systems urge us to confront these intractable problems and construct more efficient heterogeneous networks to overcome the deficiencies of current cellular networks.

1.1. Related Work

To address the aforementioned problems, many researchers are devoting their attention to designing various elaborate frameworks. Depending on the deployment method, these frameworks can be broadly classified into two groups, referred to as the static and mobile scenarios.

Static Scenario

In the static scenario, also known as the optimal placement problem, UAVs are dispatched at fixed locations to enhance the system performance.

First, the optimal displacement problem with a single UAV was studied. In [23–26], the authors determined the optimal 3-D placement of a UAV as an aerial base station to maximize the number of served ground terminals and hence improve the system sum rate. In [27,28], guidelines for the deployment of a UAV in 3-D were studied by investigating stochastic air-to-ground (A2G) channel conditions. In [29], the authors studied the joint altitude and beamwidth optimization problem for UAV-enabled multi-user communication systems. In [30], the authors investigated a multiple-input multiple-output (MIMO) framework for a UAV-assisted cellular-connected network.

Second, to further enhance the system performance, the optimization of multiple UAVs with orthogonal channels was investigated. In [31], the authors studied the minimal number of UAVs needed to seamlessly cover a fixed group of ground terminals by exploiting the characteristics of a convex hull. In [32], the authors studied the cell association problem in heterogeneous networks with UAVs as aerial base stations to assist cellular networks by exploiting optimal transport theory. In [33], the authors studied the analytical optimal displacement of UAVs with orthogonal channels by exploiting high-resolution quantization theory. In [34], the researchers studied an efficient algorithm for determining the optimal placement of multiple UAVs by jointly optimizing the resource allocation and user association while considering an in-band backhaul link.

Third, to further exploit the potential of such networks, the optimization problem for multiple UAVs with broadcast channels was investigated. In [35], the authors studied the optimal deployment of two UAVs to provide seamless service to a given area via broadcast while reducing their mutual interference. In [36], the authors studied the capacity characteristics of a UAV-enabled scenario for communication between two users via a broadcast channel. In [37], the author investigated the 3D deployment of multiple UAVs with genetic algorithm to maximize the number of the served UE. Finally, as an alternative to the broadcast approach, the authors of [38] studied an efficient algorithm for maximizing the throughput of a multi-user system by exploiting the benefits of interference among multiple UAVs in a wireless network with a coordinated multipoint (CoMP) architecture.

Mobile Scenario

Compared to static deployment, the mobile scenario is more challenging. In this scenario, the UAVs are required to provide communication services while flying along designated trajectories.

First, similar to the static scenario, the deployment of a single UAV in the mobile scenario was studied. In [39], the authors studied the delay-tolerant system performance with a UAV following a circular trajectory and a set of distributed ground terminals in the network. In [40], the authors studied the joint trajectory and power allocation problem by employing a UAV as a mobile relay to enhance the end-to-end throughput. In [41], the authors considered the optimal trajectory of a UAV acting as a relay to bridge the gap between a base station and a remote device by minimizing the outage probability. The authors of [42] studied the optimal trajectory of a UAV serving as a relay in a UAV-enabled network with a set of devices and employed the pickup and delivery method for initialization. In [43], the authors studied the optimal mobile deployment of a UAV to achieve a trade-off between coverage and delay with the coexistence of underlying device-to-device (D2D) communications in the system network. In [44,45], the authors investigated the optimal trajectories of fixed-wing and rotary-wing UAVs to achieve high throughputs while considering the energy consumption due to aerodynamics. In [46], based on the energy consumption modes mentioned above, the authors proposed an efficient trajectory programming approach for a single UAV with a certain cellular-connection constraint. In [47], based on an energy model for a fixed-wing UAV, the authors revealed a fundamental trade-off between the energy consumption of ground nodes and that of a flying base station by characterizing the Pareto front. In [48], the authors studied a solar-powered UAV-enabled system in the uplink scenario and revealed a design trade-off between the solar energy-harvesting performance and the throughput of the communication system. In [49], the authors studied the optimal trajectory of a UAV in a multi-user data collection scenario by employing a UAV equipped with multiple antennas as an aerial base collector. In [22], the authors initiated the study of the minimal completion time for data collection from sensors distributed along a fixed straight line. In [50], the minimal completion time for a UAV-enabled scenario was extended to a general model under a random linear network coding framework. In [51], the researchers considered the optimal trajectory of a mobile UAV serving as a secondary transmitter to maximize the service throughput with the coexistence of multiple licensed users in a cognitive system scenario. In [52], the authors studied optimal resource allocation and trajectory design for a UAV in a data collection scenario with an upload-time constraint. In [53], based on the characteristics of a random fading channel, the authors proposed an efficient resource allocation and trajectory programming framework for harvesting data in the IoT scenario by exploiting the advantages of multiple antennas. In [54], the authors studied the adaptive optimal UAV displacement in a network based on the distribution of users and a majority-vote rule.

Second, the use of multiple UAVs with orthogonal channels in the mobile scenario was investigated. In [21], the joint quasi-static deployment and uplink power problem for multiple UAVs in the IoT scenario was investigated for the collection of data from ground devices in the presence of interference. In [55], the authors extended the minimal completion time problem for UAV-enabled data collection to the multi-UAV case with

orthogonal channels. In [56], the authors studied the optimal trajectories of UAVs using a multi-agent Q-learning-based algorithm.

Finally, cases involving multiple UAVs with channel interference were investigated. In [57], the authors initiated the study of joint trajectory and downlink communication design for multiple UAVs with interference coordination (IC). In [58], the authors considered IC management for a multi-UAV case in the downlink scenario based on joint trajectory and power optimization. In [59], the authors studied the guidelines for designing the throughput maximization problem for two UAVs in a wireless powered scenario with channel interference. In [60], the authors summarized the previous research achievements and identified several fundamental design trade-offs associated with the application of UAVs.

1.2. The Existing Problem

Despite the above efforts, in practice, applications of UAVs for data harvesting still face numerous physical constraints, i.e., the size, weight and power limitations (SWPL) of the UAVs [57], which make it infeasible to complete certain missions by deploying a single vehicle.

Intuitively, the deployment of multiple UAVs is a direct way to overcome the above obstacles. However, numerous studies mentioned above simply consider optimizing the throughput of a system by dispatching a single UAV [22,44,49,50], and the related frameworks are, in general, inapplicable to the multi-UAV scenario due to the complicated problems related to resource allocation and interference arising from the deployment of multiple UAVs. On the other hand, some related studies have investigated the uplink scenario by exploiting the advantages of multiple UAVs, but only orthogonal channels [33,55,56] or partially orthogonal channels [21] have been considered.

To further enhance the spectral efficiency of such systems, some researchers have attempted to work on an optimal framework with channel IC. Ref. [57] introduced a framework for IC optimization by jointly considering resource allocation, power and trajectory design, but the resource allocation sub-problem was relaxed to a fractional form, and the equivalence was left unsolved. Moreover, only the downlink mode of the system was emphasized in the literature, whereas the uplink problem involves a more sophisticated association and scheduling formulation. In addition, only circular trajectory initialization was discussed in the literature, which is insufficient to determine a feasible solution in a more complicated scenario with numerous nodes distributed over an area without distinct grouping characteristics. In [59], the authors detailed the optimal displacement and trajectory problem for a wireless powered UAV system in the time-division (TD), IC and CoMP scenarios. However, this formulation simply comprised two ground nodes and two UAVs, without addressing any sophisticated grouping strategy or designs for resource allocation among numerous ground nodes; furthermore, the algorithm was not simultaneously compatible with the TD and IC scenarios; and finally, similar to previous research, no experimental results for cases with more than two UAVs were presented to demonstrate the efficiency with multiple UAVs. In [21], the authors proposed a series of sub-problems to enhance data collection in the IoT scenario by exploiting the advantages of multiple UAVs. However, a set of orthogonal channels was assumed in this scenario, and IC was considered only when the number of ground nodes exceeded the number of independent channels; in addition, the transmit power of the devices was assumed to be optimized to reduce the severity of interference in the system, but this is generally infeasible in practice due to the simplified structure of the radio frequency signals adopted by distributed sensors.

1.3. Our Contributions

In this paper, we consider the minimal completion time problem for data collection from a set of distributed sensors in the IoT scenario by exploiting the mobility of multiple UAVs operating in the same frequency band to support the network. In this setting, we provide a general joint resource allocation and trajectory design formulation that

is compatible with both the traditional TD scheme and the IC scheme and, moreover, can adapt itself to different interference conditions to optimally enhance the network throughput. The main contributions are summarized as follows.

- First, we consider the minimal completion time problem for data collection in a wireless network in which multiple UAVs are dispatched to harvest the data uploaded by a set of ground devices or sensors with shared frequency channels to improve the system efficiency. We design a general joint resource allocation and trajectory optimization formulation that can support adaptive interference management and endow the wireless network with additional system gain, flexibility and robustness compared to solely orthogonal-frequency and IC systems.
- Second, we first validate the effectiveness of the proposed algorithm in a basic network consisting of two UAVs and four aligned devices, in which the UAVs can hover at the optimal displacements to harvest the data. We prove that the minimal throughput (common throughput) of the network is non-decreasing with respect to the distance between the served devices. Building upon this insightful proposition, we further validate the effectiveness of the algorithm for the general mobile UAV scenario with extensive numerical results.
- Finally, based on the optimal resource allocation solution, we provide a metric for determining the maximum number of UAVs that can be used in our proposed algorithm to avoid serious interference affecting the completion time in practical applications.

The remainder of this paper is organized as follows. Section 2 introduces the system model of the multi-UAV-enabled wireless data collection network. Section 3 formulates the optimization problems. Section 4 presents sufficient theoretical analyses of the optimal solution to the joint resource allocation and trajectory design problem in a basic network with two UAVs and four devices. Section 5 proposes an efficient algorithm for obtaining a locally optimal solution to the joint resource allocation and trajectory design problem in the general scenario. In Section 6, numerical experimental results are presented to validate the efficiency of our proposed designs and illustrate principles of practical application. Finally, Section 7 presents the conclusions drawn from this paper.

Notations: Scalars are denoted by lower-case letters, vectors by boldface lower-case letters and matrices by boldface upper-case letters. $\mathbf{I}$ and $\mathbf{0}$ denote an identity matrix and an all-zero matrix, respectively. For a vector $\mathbf{w}$, $\|\mathbf{w}\|$ represents its Euclidean norm. For a square matrix $\mathbf{B}$, $\mathbf{B}_{i,i}$ denotes its ith diagonal element, and $\mathbf{B}^T$ denotes its conjugate transpose. $|\mathcal{U}|$ denotes the cardinality of the set $\mathcal{U}$. For a time-dependent function $g(t)$, $\dot{g}(t)$ denotes the derivative with respect to time t. The notation $\log_2(\cdot)$ denotes the logarithm function with base 2, e denotes the natural constant and $\mathbb{E}(\cdot)$ denotes the statistical expectation. The distribution of a circularly symmetric complex Gaussian (CSCG) random vector with mean y and covariance matrix Ω is denoted by $\mathcal{CN}(y, \Omega)$, and $\sim$ stands for "distributed as".

2. System Model

As shown in Figure 1, in this paper, we consider an uplink wireless UAV-enabled data collection network, in which $N > 1$ rotary-wing UAVs with one antenna are dispatched to collect the data uploaded by a set of $U > 1$ distributed devices with one antenna; we consider only the case of $U > N$, and the sets of UAVs and devices are denoted by $\mathcal{N}$ and $\mathcal{U}$, respectively, with $|\mathcal{N}|=N$ and $|\mathcal{U}|=U$.

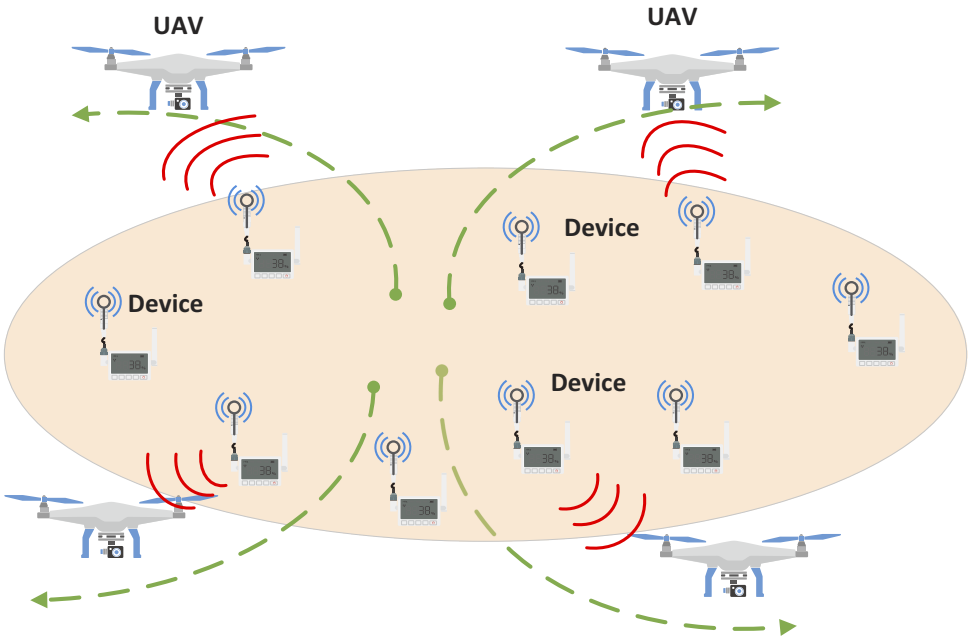

Figure 1. The multi-unmanned aerial vehicle (UAV)-enabled data collection scenario with channel interference, where multiple UAVs are flying in the sky to collect data from served devices and numerous sensors distributed over an area at fixed locations during a certain period. The dotted green lines represent the trajectories of the UAVs.

To further exploit the potential of this UAV-enabled network, we assume that all communication channels between the devices and UAVs share the same frequency band in the network over the total completion time $T > 0$, expressed in seconds, where the completion time T is an objective to be minimized and we denote the set of working times by $\mathcal{T}=\{t|0 \leq t \leq T\}$. Here, we assume that devices in the scenario are all access-time-delay-tolerant nodes, an assumption that is applicable in the majority of situations in the IoT context, in which sensors collect data, save the collected data in their caches and upload data periodically.

As a result that multiple UAVs are dispatched for improved efficiency, in this scenario, we assume that all N devices are first grouped into clusters with similar equivalent workloads, denoted by $\mathcal{G}$, where the number of groups is assumed to be equal to the number of UAVs; thus, we have $|\mathcal{G}|=|\mathcal{N}| = N$ and $\mathcal{G}= \bigcup_{n=1}^{N} \mathcal{G}_n$. Furthermore, we define binary variables $g_{n,u} \in \{0,1\}$, with $n \in \mathcal{N}$ and $u \in \mathcal{U}$, as the elements of the group association matrix, where $g_{n,u}=1$ indicates that device u is associated with cluster n and $g_{n,u}=0$ otherwise, and the set representing the nth group is denoted by $\mathcal{G}_n = \{u|g_{n,u} = 1, u \in \mathcal{U}\}$. Moreover, we use $\mathcal{G}^{-1}(u)$ to denote the index of the group to which the uth device belongs. A good grouping strategy will lead to higher-quality performance of the system, and we will detail the grouping process below. As a result that the same channel frequency is shared among all devices in the network and only one antenna is mounted on each UAV, we assume that at each working time $t \in T$, at most one device can be associated with the nth UAV, and at most one UAV can be simultaneously scheduled to a corresponding paired ground device. A multi-antenna-equipped system could further enhance the network capabilities, as detailed in [53], but this would require a more complicated strategy for the multi-UAV scenario and is left as a subject for future study.

To mathematically formulate the above physical description of the system, we define binary variables $\alpha_{n,u}(t) \in \{0,1\}$ as the elements of the association and scheduling matrix at time $t \in T$, where $\alpha_{n,u}(t)=1$ indicates that device u is associated with UAV n and UAV n is simultaneously scheduled to device u; otherwise, $\alpha_{n,u}(t)= 0$. Moreover, we use

$b_u(t) \in \{0,1\}$ to denote the state of transmission for each device, where $b_u(t)$=1 indicates that device u is active; otherwise, the device is inactive.

Without loss of generality, we consider a 3-D Cartesian coordinate system, in which the horizontal coordinates of device u are denoted by $\mathbf{w}_u = [x_u, y_u]^T \in \mathbb{R}^{2\times 1}$, $u \in \mathcal{U}$. We assume that the horizontal coordinates of the devices are fixed during each mission period and can be perfectly obtained by the network prior to the mission. We note that the above assumption is applicable in the IoT scenario in general, as the positions of sensors are relatively static within a single period and the coordinates of each sensor can be promptly updated by means of the Global Positioning System (GPS) [61,62].

In this paper, all UAVs are assumed to fly at a constant altitude H. We note that freedom of altitude could help to alleviate interference and enhance the system performance, as detailed in [51]; however, frequent vertical movements of a UAV may lead to considerable aerodynamic energy consumption [45], which may be several orders of magnitude greater than its electrical counterpart. Thus, the effects of altitude adjustments on the system should be thoroughly investigated from the perspectives of communication requirements and energy efficiency, and this is left as a topic of future study.

Furthermore, the horizontal coordinates of each UAV $n \in \mathcal{N}$ in any time slot $t \in \mathcal{T}$ are denoted by $\mathbf{q}_n(t) = [x_n(t), y_n(t)]^T \in \mathbb{R}^{2\times 1}$, $t \in \mathcal{T}$, and the distance from UAV n to user u at time t can be expressed as $d_{n,u}(t) = \sqrt{\|\mathbf{q}_n(t) - \mathbf{w}_u\|^2 + H^2}$, $\forall n \in \mathcal{N}, \forall u \in \mathcal{U}$. Without loss of generality, we assume that the drones are constrained by several practical limitations, such as take-off position constraints $\mathbf{q}^I = [\mathbf{q}_1^I, \cdots, \mathbf{q}_N^I]$, with $\mathbf{q}_n^I = [x_n^I, y_n^I]^T \in \mathbb{R}^{2\times 1}$; landing point constraints $\mathbf{q}^F = [\mathbf{q}_1^F, \cdots, \mathbf{q}_N^F]$, with $\mathbf{q}_n^F = [x_n^F, y_n^F]^T \in \mathbb{R}^{2\times 1}$; a maximal velocity constraint $V \le V_{\max}$; and a minimal distance $d_{\min}$ between drones to avoid collision during flight. Thus, we have the following constraints:

$$\|\dot{\mathbf{q}}(t)\| \le V_{\max} \tag{1}$$

$$\|\mathbf{q}_i(t) - \mathbf{q}_j(t)\| \ge d_{\min}, \forall i, j \in \mathcal{N}, i \ne j \tag{2}$$

$$\mathbf{q}_n(0) = \mathbf{q}_n^I,\ \mathbf{q}_n(T) = \mathbf{q}_n^F,\ n \in \mathcal{N} \tag{3}$$

Similar to [38,49,50], for high-altitude UAVs, we assume that the uplinks from the devices to the UAVs exhibit Rician fading channel characteristics with a large Rician factor, mainly consisting of two parts: a LoS-deterministic part and a random part following a Rayleigh distribution. The equivalent baseband channel can be formulated as follows:

$$\tilde{h}_{n,u}(t) = \sqrt{\frac{\beta_0}{d_{n,u}(t)^\alpha}}\left(\sqrt{\frac{R}{R+1}}e^{j\theta_{n,u}(t)} + \sqrt{\frac{1}{R+1}}z_{n,u}(t)\right), \forall n \in \mathcal{N}, \forall u \in \mathcal{U} \tag{4}$$

where R denotes the Rician factor and $h_{n,u}(t) = \left|\tilde{h}_{n,u}(t)\right|^2$ denotes the path loss of the power channel, with α being the path loss exponent. Moreover, β_0 denotes the channel power gain at a reference distance of $d_0 = 1$ m, and $\theta_{n,u}(t) = \frac{2\pi}{\lambda}d_{n,u}(t)$ indicates the instantaneous phase of the channel between UAV n and the corresponding ground device u, with $\lambda = \frac{c}{f_c}$ denoting the wavelength, where c is the speed of light and f_c is the carrier frequency. Finally, $z_{n,u}(t)$ is a CSCG random variable with zero mean and unit variance.

Remark: We notice that the probabilistic A2G model proposed in [63] has been adopted in various literatures. The fundamental difference between the probabilistic channel model and Rician channel adopted in this paper is that the elevation angel exerts a subtle influence on the receiving power at the receiver for the probabilistic A2G channel. In our scenario, the inter-interference arising from co-working device is the key point to be carefully controlled to avoid compromising the performance of the network. Based on the proof given in [21], the LOS dominant channel gives the upper bound on the amount of inter-interference power compared the mixed LOS and NLOS channel. On the other hand, a well group strategy is adopted in this paper, thus, the elevation angle between the

serving device and serving UAV is large enough to have a LOS dominant channel between the paired device and receiver (i.e., UAV). Based on above two factors, the channel adopted in this paper gives the upper bound of the completion time compared to the probabilistic G2A model, although the tightness of the bound is left for our future work.

According to the above assumptions, the locations of all the ground devices are perfectly known to the UAVs; however, instantaneous channel state information (CSI) may not be available due to the fast randomness caused by the Rayleigh distribution. Thus, only statistical CSI is assumed to be exploited in this paper.

To fully exploit the potential of the system and minimize the mission completion time, the flying data collection scheme defined in [55] is adopted to deploy the UAVs, which means that the designated drones continuously provide bridging communication links with their paired devices while flying along their preset trajectories. To avoid Doppler effects during flight, the gain loss is assumed to be well compensated at the receiver with Doppler estimation and synchronization techniques [64].

In contrast to [21], we assume that the transmit power of the ground devices is constant and equal among all devices, denoted by p_u, $u \in \mathcal{U}$. Thus, the corresponding received signal-to-interference-plus-noise ratio (SINR) at UAV n when UAV n is linked to ground device u can be expressed as follows:

$$\gamma_{n,u}(t) = \frac{p_u b_u(t) h_{n,u}(t)}{I_n(t) + \sigma^2}, \forall t \in \mathcal{T} \tag{5}$$

where σ^2 is the power of the additive white Gaussian noise (AWGN) at the receiver and $I_n(t)$ denotes the instantaneous interference at UAV n caused by the active devices linked to other UAVs j, $j \in \mathcal{N} \backslash \{n\}$, and can be formulated as follows:

$$I_n(t) = \sum_{\substack{j=1 \\ j \neq n}}^{N} \sum_{w \in \mathcal{G}_j} \alpha_{j,w}(t) b_w(t) p_w h_{n,w}(t), \forall t \in \mathcal{T} \tag{6}$$

Based on the above series of assumptions and models, the instantaneous achievable rate of ground device u linked to UAV n in bits per second (bps) can be formulated as

$$\tilde{R}_{n,u}(t) = B \log_2(1 + \gamma_{n,u}(t)) \tag{7}$$

where B denotes the bandwidth of the network measured in hertz. To meet the data collection requirement of each device u, we have the following communication constraint:

$$\int_0^T \sum_{n=1}^{N} g_{n,u} \alpha_{n,u}(t) \tilde{R}_{n,u}(t) \geq D_u, \quad \forall u \in \mathcal{U} \tag{8}$$

where D_u is a constant value representing the size of the data that should be collected from device u by a scheduled UAV within one time period T.

The instantaneous rate $\tilde{R}_{n,u}(t)$ is a random variable due to the randomness of the Rayleigh channel, and in this paper, we are interested only in the expected rate; thus, the presented framework represents an offline design. However, in practice, $\tilde{R}_{n,u}(t)$ can be equivalent to the difference between two concave functions; thus, the instantaneous rate is neither a convex function nor a concave function with respect to the channel power gain $h_{n,u}$. To make the expression more tractable, similar to the approach in [49], we take the following approximation and denote the approximate instantaneous rate by $R_{n,u}(t)$:

$$\mathbb{E}\{\tilde{R}_{n,u}(t)\} \simeq B \log_2(1 + \mathbb{E}\{\gamma_{n,u}(t)\}) = R_{n,u}(t) \tag{9}$$

$$R_{n,u}(t) = B\log_2\left(1+\frac{p_u(t)\underset{h_{n,u}}{\mathbb{E}}\{h_{n,u}(t)\}}{\underset{\substack{h_{i,u}\\ i\neq n}}{\mathbb{E}}\{I_n(t)\}}\right) = B\log_2\left(1+\frac{p_u(t)\beta_0 d_{n,u}^{-\alpha}}{\sum_{\substack{j=1\\ j\neq n}}^{N}\sum_{\omega\in\mathcal{G}_j} p_\omega \alpha_{j,\omega}(t)\beta_0 d_{n,\omega}^{-\alpha}+\sigma^2}\right) \tag{10}$$

The above approximation offers remarkable accuracy with a sufficiently large Rician factor, a requirement that is generally satisfied in UAV communication scenarios [49]. Based on the above assumption, we focus on optimizing the approximate expected rate $R_{n,u}(t)$ instead.

3. Problem Formulation

Our target is to minimize the completion time of a data collection mission in the spectrum sharing scenario by jointly coordinating grouping, resource allocation and trajectory design among the multiple UAVs while considering the data requirements and energy limitations of each ground device. The optimization problem can be formulated as P1 below:

$$\begin{aligned}
(\mathrm{P1}): \min_{\{\mathcal{G},\mathbf{Q},\mathbf{A},\mathbf{B},T\}} \quad & T \\
\text{s.t.} \quad & \alpha_{n,u}(t)\in\{0,1\}, && \forall n\in\mathcal{N},\forall u\in\mathcal{U},\forall t\in\mathcal{T} && (11)\\
& \sum_{n=1}^{N} g_{n,u}\alpha_{n,u}(t)\le 1, && \forall n\in\mathcal{N},\forall u\in\mathcal{U},\forall t\in\mathcal{T} && (12)\\
& \sum_{u=1}^{U} g_{n,u}\alpha_{n,u}(t)\le 1, && \forall n\in\mathcal{N},\forall u\in\mathcal{U},\forall t\in\mathcal{T} && (13)\\
& b_u(t)\in\{0,1\}, && \forall u\in\mathcal{U},\forall t\in\mathcal{T} && (14)\\
& \int_0^T \sum_{n=1}^{N} g_{n,u}\alpha_{n,u}(t)b_u(t)p_u \le E_u && \forall u\in\mathcal{U} && (15)\\
& \int_0^T \sum_{n=1}^{N} g_{n,u}\alpha_{n,u}(t)b_u(t)R_{n,u}(t) \ge D_u && \forall u\in\mathcal{U} && (16)\\
& (1),(2) \text{ and } (3) && && (17)
\end{aligned}$$

where $\mathbf{Q}$, $\mathbf{A}$ and $\mathbf{B}$ are the sets of all $\mathbf{q}_n(t)$, $\alpha_{n,u}(t)$ and $b_u(t)$.

Constraint (12) indicates that only one UAV can be scheduled to one device in a single slot. Constraint (13) means that only one user can be associated with one UAV at a time. Constraint (15) limits the maximum energy consumption for uploading by any device over the completion time. Constraint (16) represents the data upload requirements of each device.

Note that P1 is a continuous optimization problem with infinite variables and is difficult to solve with a numerical approach; hence, P1 needs to be discretized with a sufficient number of time slots, and accordingly, we denote the duration of a single time slot and the set of all time slots by δt and $\mathcal{M}$, respectively, with $M = |\mathcal{M}|$. Moreover, extensive research has yielded a principle for determining an appropriate time slot duration to strike a balance between accuracy and computational efficiency, i.e., $V_{\max}\delta t \ll H$. For the spectrum sharing scenario, the contributors to the interference within each time slot should be clarified; otherwise, the physical meaning of the problem will be poorly defined. In addition, we assume that the association and scheduling operations take a certain amount of time, which cannot be treated as infinitesimal in general, as frequent switching operations on the devices will lead to considerable energy consumption of the circuits, resulting in power inefficiency of the devices. Hence, for simplicity, we assume that a single association and scheduling period is characterized by an interval similar to the

time slot duration δt, and accordingly, we introduce variables $b_u[m] \in [0,1]$ to represent the percentage of working time between the nth UAV and the uth device within the mth time slot. Then, we apply Jensen's inequality and obtain a lower bound on the expected rate as follows, where the inequality holds because $b_u(t) \in \{0,1\}$:

$$\begin{aligned} R_{n,u}(t) &= B\log_2\left(1+\frac{b_u(t)p_u\beta_0 d_{n,u}^{-\alpha}}{\sum_{\substack{j=1\\ j\neq n}}^{N}\sum_{\omega\in\mathcal{G}_j}p_\omega(t)\alpha_{j,\omega}(t)\beta_0 d_{n,\omega}^{-\alpha}+\sigma^2}\right) \\ &\geq Bb_u(t)\log_2\left(1+\frac{p_u\beta_0 d_{n,u}^{-\alpha}}{\sum_{\substack{j=1\\ j\neq n}}^{N}\sum_{\omega\in\mathcal{G}_j}p_\omega(t)\alpha_{j,\omega}(t)\beta_0 d_{n,\omega}^{-\alpha}+\sigma^2}\right) \triangleq b_u(t)R_{n,u}^{lb}(t) \end{aligned} \tag{18}$$

where $R_{n,u}^{lb}[m] = B\log_2\left(1+\frac{p_u\beta_0 d_{n,u}^{-\alpha}}{\sum_{\substack{j=1\\ j\neq n}}^{N}\sum_{\omega\in\mathcal{G}_j}p_\omega b'_\omega[m]\alpha'_{j,\omega}[m]\beta_0 d_{n,\omega}^{-\alpha}+\sigma^2}\right)$.

Thus, the original problem can be represented as P2 below:

$$(\mathrm{P2}): \min_{\{\mathcal{G},\mathbf{Q}',\mathbf{A}',\mathbf{B}',M\}} M$$

$$\text{s.t.} \quad \alpha'_{n,u}[m] \in \{0,1\}, \qquad \forall n\in\mathcal{N}, \forall u\in\mathcal{U}, m\in\mathcal{M} \tag{19}$$

$$\sum_{n=1}^{N} g_{n,u}\alpha'_{n,u}[m] \leq 1, \qquad \forall n\in\mathcal{N}, \forall u\in\mathcal{U}, m\in\mathcal{M} \tag{20}$$

$$\sum_{u=1}^{U} g_{n,u}\alpha'_{n,u}[m] \leq 1, \qquad \forall n\in\mathcal{N}, \forall u\in\mathcal{U}, m\in\mathcal{M} \tag{21}$$

$$0 \leq b'_u[m] \leq 1, \qquad \forall u\in\mathcal{U}, m\in\mathcal{M} \tag{22}$$

$$\sum_{m=1}^{M}\sum_{n=1}^{N} g_{n,u}b'_u[m]\alpha'_{n,u}[m]p_u \leq E_u/\delta t, \qquad \forall u\in\mathcal{U}, m\in\mathcal{M} \tag{23}$$

$$\sum_{m=1}^{M}\sum_{n=1}^{N} g_{n,u}b'_u[m]\alpha'_{n,u}[m]R_{n,u}^{lb}[m] \geq D_u/\delta t, \qquad \forall u\in\mathcal{U}, m\in\mathcal{M} \tag{24}$$

$$\left\|\mathbf{q}'_i[m]-\mathbf{q}'_j[m]\right\| \geq d_{\min}, \qquad \forall i,j\in\mathcal{N}, i\neq j, m\in\mathcal{M} \tag{25}$$

$$\left\|\mathbf{q}'_n[m+1]-\mathbf{q}'_n[m]\right\| \leq V_{\max}\cdot\delta t, \qquad \forall n\in\mathcal{N}, m\in\mathcal{M} \tag{26}$$

$$\mathbf{q}'_n[0]=\mathbf{q}_n^I, \mathbf{q}'_n[M]=\mathbf{q}_n^F, \qquad \forall n\in\mathcal{N} \tag{27}$$

where $\mathbf{Q}'$ and $\mathbf{A}'$ are the sets of all $\mathbf{q}'_n[m]$ and $\alpha'_{n,u}[m]$, respectively, and accordingly, $\mathbf{B}'$ is the set of all $b'_u[m]$.

We note that P2 encompasses not only the IC scheme, under which there are different active devices within the same slot, but also the TD scheme, under which only one device is linked at a time. Therefore, the TD and IC schemes are both simply special cases of P2, which means that the above model allows adaptive adjustment of the strategy according to the severity of interference. Table 1 lists the different possible schemes along with their corresponding parameters.

Table 1. Illustration of schemes with different parameters.

Scheme	$\alpha_{n,u}[m]$	$b_{n,u}[m]$
Interference coordination (IC)	$\zeta = N$ different devices are active during the mth time slot	$b_{n,u}[m] = \begin{cases} 1, & \alpha_{n,u}[m] = 1, \forall n \in \mathcal{N}, \forall u \in \mathcal{U} \\ 0, & \text{otherwise} \end{cases}$
IC/TD hybrid scheme	$1 < \zeta < N$ different devices are active during the mth time slot	$\begin{cases} b_{n,u}[m] \in (0,1], \alpha_{n,u}[m] = 1, \forall n \in \mathcal{N}, \forall u \in \mathcal{U} \\ b_{n,u}[m] = 0, \quad \text{otherwise} \end{cases}$
Time division(TD)	Only $\zeta = 1$ device is active	$b_{n,u}[m] = \begin{cases} 1, & \alpha_{n,u}[m] = 1, \forall n \in \mathcal{N}, \forall u \in \mathcal{U} \\ 0, & \text{otherwise} \end{cases}$

According to [42,55], the completion formulation P2 is equivalent to the following optimization problem P3 with two sub-problems. Specifically, P3-1 is a univariate optimization problem and can be solved efficiently with the 1-D bisection approach because of the monotonicity of $\eta^*(M)$. Hence, in the following sections, we focus on how to solve the non-convex problem P3-2 efficiently.

$$(\text{P3}-1): \min_{\eta} \quad M$$
$$\text{s.t.} \quad \eta^*(M) \geq 1 \tag{28}$$

$$(\text{P3}-2): \min_{\{\mathcal{G}, \mathbf{Q}', \mathbf{A}', \mathbf{B}'\}} \quad \eta$$
$$\text{s.t.} \quad \frac{\delta t}{D_u} \sum_{m=1}^{M} \sum_{n=1}^{N} g_{n,u} b'_u[m] \alpha'_{n,u}[m] R^{lb}_{n,u}[m](t) \geq \eta \quad \forall u \in \mathcal{U} \tag{29}$$
$$(19)-(23), (25)-(27) \tag{30}$$

4. Analysis for a Basic Network Scenario

In [36], the authors revealed the effects of the velocity and time duration on the network capacity between two users and a single UAV when the UAV collects data from the two users simultaneously and achieves a trade-off in the terminal requirements, and they reported that the Pareto front for the system capacity is achieved when the velocity of the vehicle is infinite. To investigate the trend of change for the optimal resource strategy in our considered scenario, in this section, we will first study a basic network consisting of only two UAVs and four ground devices, where the velocity of the UAVs is sufficiently high that the UAVs can hover at the optimal displacements to harvest data from the devices, as shown in Figure 2. Without loss of generality, the four devices are symmetrically distributed along the x axis at distances of L_1 and L_2 from the origin, where we assume that $L_2 > L_1 > d_{\min}$.

To make the problem more tractable and obtain an insightful solution, we assume that each device has equal data requirements $D_u = D, \forall u \in \mathcal{U}$, and set the path loss exponent to $\alpha = 2$. Furthermore, we assume that in this scenario, the signal-to-noise ratio (SNR) or interference-to-noise ratio (INR) at the receiver is much greater than 1.

This basic network consists of two basic elements, each composed of two UAVs and two devices that are symmetrically distributed along the axis. While the nature of this basic element has been detailed in [59], here, we extend this work to the basic network scenario presented above. First, we present a lemma to characterize the aforementioned basic element.

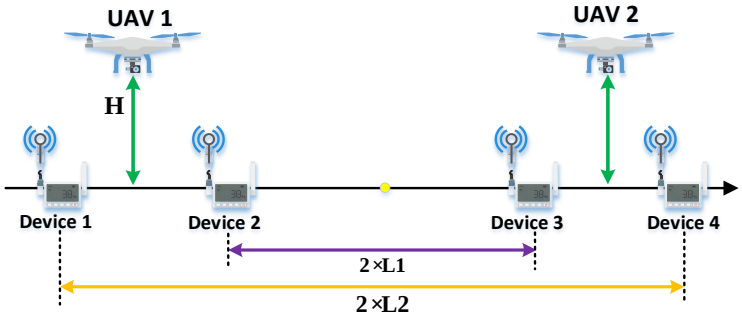

Figure 2. A basic network scenario with two UAVs and four devices, where the four devices are symmetrically distributed along a line and the two UAVs fly at a constant height to collect data from their served devices.

Lemma 1. *The optimal hovering placement x^* of the two UAVs with channel interference is tightly upper bounded by $\sqrt{(L/2)^2+H^2}$, where L denotes the distance between the two devices.*

Proof. For two UAVs and two devices in the IC case, the optimal horizontal hovering points should satisfy the following equation [59]:

$$\frac{(x^*+L/2)\left((x^*-L/2)^2+H^2\right)^2}{\beta_0 p_u/\sigma^2}-L\left(H^2+\left(\frac{L}{2}\right)^2-(x^*)^2\right)=0,\ x^*\in\left[\frac{L}{2},\sqrt{(L/2)^2+H^2}\right] \tag{31}$$

$$\Rightarrow\left(H^2+\left(\frac{L}{2}\right)^2-(x^*)^2\right)=\frac{\left(x^*+\frac{L}{2}\right)\left(\left(x^*-\frac{L}{2}\right)^2+H^2\right)^2}{L\beta_0 p_u/\sigma^2},\quad x^*\in\left[\frac{L}{2},\sqrt{(L/2)^2+H^2}\right] \tag{32}$$

where L denotes the distance between the two ground devices assigned to separate drones. Based on the above equation, we can derive a tight upper bound on the distance between the optimal hovering points as follows:

$$\begin{aligned}&\Rightarrow (S-x^*)L<(S+x^*)(S-x^*)\le\frac{\left(S+\frac{L}{2}\right)\left(\left(S-\frac{L}{2}\right)^2+H^2\right)^2}{L\beta_0 p_u/\sigma^2}\\&\Rightarrow d\le\frac{\left(S+\frac{L}{2}\right)\left(\left(S-\frac{L}{2}\right)^2+H^2\right)^2}{L^2\beta_0 p_u/\sigma^2}\end{aligned} \tag{33}$$

where $S\triangleq\sqrt{H^2+(L/2)^2}$ and $d\triangleq S-x^*$. Moreover, we have the following inequality with respect to S and L:

$$S^2=(L/2)^2+H^2<(L/2+H)^2\Rightarrow S-L/2<H \tag{34}$$

Plugging this inequality into (33), we obtain

$$\Rightarrow d\le\frac{\left(S+\frac{L}{2}\right)\left(\left(S-\frac{L}{2}\right)^2+H^2\right)^2}{L^2\beta_0 p_u/\sigma^2}<\frac{4\sigma^2H^2(L+H)}{L^2\beta_0 p_u}\xrightarrow{L\to\infty}0 \tag{35}$$

Thus, the optimal hovering placement x^* of the two UAVs for two devices with channel interference is tightly upper bounded by $\sqrt{(L/2)^2+H^2}$. The proof is complete. □

Lemma 1 indicates that the optimal hovering locations for a basic element can be approximated by a closed-form expression with satisfactory accuracy. Furthermore, based on Lemma 1, we can draw an insightful conclusion about the considered basic element, as given in Lemma 2.

Lemma 2. *The optimal common throughput for data collection from the network in the two-UAV, two-device scenario is non-decreasing with respect to the distance L between the two devices, and the minimal common throughput for this basic element is lower bounded by the TD scheme.*

Proof. As discussed previously, the scheme adopted in the system can be adjusted between the TD and IC modes. The communication rate depends only on the UAV height when the TD mode is applied, which means that the optimal rate performance of the system is no less than that under the TD scheme. When the two devices are very close to each other, the interference on each receiver arising from the co-working devices is strong; thus, the TD scheme should be employed to optimally harvest data in such an element, and the system should be switched from the TD mode to the IC mode only when the separation distance is sufficient.

We assume that when the distance between the two UAVs is $L^{\dagger}$, the two UAVs operating in the TD mode have the same capacity as in the IC mode with the corresponding optimal hovering locations. It is obvious that the optimal hovering point for a UAV in the TD scheme is just above the corresponding device, and the optimal hovering location for the IC mode can be approximated in closed form as shown in Lemma 1. Thus, we have the following equality:

$$\underbrace{\log\left(1+\frac{\frac{\beta_0 p_u}{\left(x^*-L^{\dagger}/2\right)^2+H^2}}{\frac{\beta_0 p_u}{\left(x^*+L^{\dagger}/2\right)^2+H^2}+\sigma^2}\right)}_{\text{rate for IC case}}=\underbrace{\frac{1}{2}\log\left(1+\frac{\beta_0 p_u}{H^2\sigma^2}\right)}_{\text{rate for TD case}} \tag{36}$$

where $x^* \simeq \sqrt{\left(L^{\dagger}/2\right)^2+H^2}$. Under the assumption that the SNR is sufficiently large, we have the following equation:

$$\begin{aligned}
&\Rightarrow \sqrt{\frac{\beta_0 p_u}{H^2\sigma^2}}=1+\frac{\frac{\beta_0 p_u}{\left(x^*-L^{\dagger}/2\right)^2+H^2}}{\frac{\beta_0 p_u}{\left(x^*+L^{\dagger}/2\right)^2+H^2}}=\frac{2H^2+\left(x^*+L^{\dagger}/2\right)^2+\left(x^*-L^{\dagger}/2\right)^2}{\left(x^*-L^{\dagger}/2\right)^2+H^2}\\
&\Rightarrow \sqrt{\frac{\beta_0 p_u}{H^2\sigma^2}}\left[\varsigma^2+H^2\right]=4H^2+\left(L^{\dagger}\right)^2
\end{aligned} \tag{37}$$

where $\varsigma \triangleq \sqrt{\left(L^{\dagger}/2\right)^2+H^2}-L^{\dagger}/2$, and furthermore, we can give the following analytical expression for ς:

$$\begin{aligned}
&\Rightarrow \varsigma^2+L\varsigma-H^2=0\\
&\Rightarrow \varsigma=\frac{-L+\sqrt{L+4H^2}}{2}=\frac{2H^2}{L+\sqrt{L+4H^2}}
\end{aligned} \tag{38}$$

We note that ς is monotonically decreasing with respect to L and that the left-hand side of the equation is a decreasing function, while the right-hand side of the equation is an increasing function; thus, the optimal distance $L^{\dagger}$ can be efficiently obtained by means of the 1-D bisection search method. Specifically, under the high SNR and INR assumption ($SNR, INR \gg 1$), we can easily prove that $L^{\dagger} > 2H$, as the rate under the IC scheme can be represented as follows when $L = 2H$:

$$R_{L=2H}^{IC} = \log_2\left\{\frac{4H^2+L^2}{\left(x^*-\frac{L}{2}\right)^2+H^2}\right\} \overset{L=2H}{\longrightarrow} \log_2\left\{\frac{4H^2+L^2}{\left(x^*-\frac{L}{2}\right)^2+H^2}\right\} = \log_2\left\{\frac{8}{7-2\sqrt{5}}\right\} \tag{39}$$

In contrast, for the TD scheme with two UAVs, we have

$$R_{L=2H}^{TD} = \frac{1}{2}\log_2\left(\frac{\beta_0 p_u}{\sigma^2 H^2}\right) > \log_2(\sqrt{10}) > R_{L=2H}^{IC} \tag{40}$$

Based on the above derivations, the common throughput of the system is strictly increasing when $L > L^\dagger$ and is constant when $L \le L^\dagger$. □

According to Lemma 2, the optimal resource association and scheduling scheme for the basic element is simply related to the distance between the two devices. Furthermore, by combining Lemma 1 and Lemma 2, we can investigate the characteristics of the basic network scenario and present the insightful Proposition 1 given below.

Proposition 1. *The optimal resource allocation and trajectory solution for the basic network consisting of two UAVs and four symmetrically distributed devices, as shown in Figure 2, is related only to the distribution of the devices. Depending on the device distribution, the possible solutions can be divided into five different cases as follows, where* $T_1^* \ge T_2^* \ge T_3^* \ge T_4^* \ge T_5^*$.

- *Case 1: If* $2L_2 < L^\dagger$, *where* $L^\dagger$ *is given in Lemma 2, then the system will adopt the TD scheme over the entire completion time. We have* $T_1^* = 4D_u / \left(B\log_2\left(1+\frac{\beta_0 p_u}{H^2\sigma^2}\right)\right)$, *and the optimal solution to the resource allocation and hovering displacement problem can be described as follows. The total completion time is separated into four time intervals of equal duration, during each of which only one device is permitted to access the network, and the optimal hovering placement is just above the corresponding served device.*
- *Case 2: If* $2L_2 \ge L^\dagger$ *and* $L_2+L_1 < L^\dagger$, *then the minimal completion time for the basic network satisfies*

$$T_2^* = \frac{2D_u}{B\log_2\left(1+\frac{\beta_0 p_u}{H^2\sigma^2}\right)} + \frac{D_u}{B\log_2\left(1+\frac{\beta_0 p_u / \left(\left(x_1^*-L_2\right)^2+H^2\right)}{\beta_0 p_u / \left(\left(x_1^*+L_2\right)^2+H^2\right)+\sigma^2}\right)} \tag{41}$$

and the optimal solution to the resource allocation and hovering placement problem can be described as follows. During the first interval, $\left(0, T_{21}^*\right]$, *where* $T_{21}^* = 2D_u / \left(B\log_2\left(1+\frac{\beta_0 p_u}{H^2\sigma^2}\right)\right)$, *the network adopts the TD scheme; UAV 1 will be associated with device 2, hovering at* $[-x_2, 0]$, *and symmetrically, UAV 2 will be associated with device 3, hovering at* $[x_2, 0]$ *separately for half of the interval,* $T_{21}^*/2$. *In the second time interval, the system adopts the IC scheme; UAV 1 will be associated with device 1 and collect data while hovering at* $\left[-x_1^*, 0\right]$, *and simultaneously, UAV 2 will be associated with device 4 and harvest data at* $\left[x_1^*, 0\right]$, *where* $x_1^* \simeq \sqrt{L_2^2+H^2}$.
- *Case 3: If* $L'' \ge 2L_2 > L^\dagger$, $L_2+L_1 \ge L^\dagger$ *and* $2L_1 < L^\dagger$, *where the expression for* L'' *is given in the proof, then the minimal completion time and optimal solution will be the same as in case 2; thus, the description is omitted here for brevity.*
- *Case 4: If* $2L_2 \ge L''$, $L_2+L_1 > L^\dagger$ *and* $2L_1 < L^\dagger$, *then the minimal completion time is expressed as follows:*

$$T_4^* = \frac{2D_u}{B\log_2\left(1+\frac{\beta_0 p_u / \left(\left(x_3^*-x_2\right)^2+H^2\right)}{\beta_0 p_u / \left(\left(x_3^*+x_1\right)^2+H^2\right)+\sigma^2}\right)} \tag{42}$$

The optimal resource allocation solution is unique only if the serving order is not considered; based on this fact, the optimal solution to the resource allocation and hovering placement problem should satisfy the following description. During the first interval, $\left(0, T_4^*/2\right]$*, the system adopts the IC scheme; UAV 1 will be associated with device 1 and collect data while hovering at* $\left[-x_4^*, 0\right]$*, and simultaneously, UAV 2 will be associated with device 3 and harvest data at* $[x_3^*, 0]$*, where* x_3^* *and* x_4^* *are given in the proof. During the second interval, the system also adopts the IC scheme; UAV 1 will be associated with device 2 and collect data while hovering at* $[-x_3^*, 0]$*, and simultaneously, UAV 2 will be associated with device 4 and harvest data at* $\left[x_4^*, 0\right]$*.*

- *Case 5: If* $2L_1 > L^{\dagger}$*, then the system will adopt the IC scheme over the entire completion time, and we have* $T_5^* = \min(T_6, T_7)$*, where*

$$T_6 = \frac{D_u}{B\log_2\left(1+\frac{\beta_0 p_u/\left(\left(x_1^*-L_2\right)^2+H^2\right)}{\beta_0 p_u/\left(\left(x_1^*+L_2\right)^2+H^2\right)+\sigma^2}\right)} + \frac{D_u}{B\log_2\left(1+\frac{\beta_0 p_u/\left(\left(x_2^*-L_1\right)^2+H^2\right)}{\beta_0 p_u/\left(\left(x_2^*+L_1\right)^2+H^2\right)+\sigma^2}\right)} \tag{43}$$

$$T_7 = \frac{2\times D_u}{B\log_2\left(1+\frac{\beta_0 p_u/\left(\left(x_3^*-(L_1+L_2)/2\right)^2+H^2\right)}{\beta_0 p_u/\left(\left(x_3^*+(L_1+L_2)/2\right)^2+H^2\right)+\sigma^2}\right)} \tag{44}$$

  - *When* $T_5^*=T_6$*, the optimal solution to the resource allocation and hovering placement problem is described as follows. During the first interval,* $\left(0, T_{51}\right]$*, the system adopts the IC scheme; UAV 1 will be associated with device 1 and hover at* $\left[-x_2^*, 0\right]$ *to collect data, and simultaneously, UAV 2 will be associated with device 3 and harvest data at* $[x_2^*, 0]$*. Here,*

$$T_{51} = \frac{D_u}{B\log_2\left(1+\frac{\beta_0 p_u/\left(\left(x_2^*-L_1\right)^2+H^2\right)}{\beta_0 p_u/\left(\left(x_2^*+L_1\right)^2+H^2\right)+\sigma^2}\right)} \tag{45}$$

    During the second time interval, $\left(T_{51}^*, T^*\right]$*, the system also adopts the IC scheme; UAV 1 will be associated with device 1 and hover at* $\left[-x_1^*, 0\right]$ *to collect data, and simultaneously, UAV 2 will be associated with device 3 and harvest data at* $\left[x_1^*, 0\right]$*.*
  - *When* $T_5^*=T_7$*, the optimal solution to the resource allocation and hovering placement problem is the same as in case 4; thus, the description is omitted here for brevity.*

Proof. Refer to Appendix A. □

According to Proposition 1, with increasing distance between the devices, the optimal resource allocation scheme for the network switches from the TD scheme to the IC scheme; this is compatible with Lemma 2, in which only two devices are considered. Specifically, for case 1, in which all devices are gathered together with a small spacing, only one device is active and permitted to access the wireless network at any given time throughout the completion time; hence, the effect of the multiple UAVs is equivalent to that of only a single vehicle, and therefore, the efficiency of the network is low. More insightful analyses of the number of UAVs will be presented in combination with simulation results in the last section of this paper. For the other cases, the common throughput of the network is related to the interference conditions, which vary with different distributions of the devices, thus leading to different collection times. We note that if the devices are initialized with equal time resources, the network will allocate more resources to devices that are subject to more serious interference to minimize the system completion time.

5. Joint Optimization for the General Mobile Problem

In this section, we investigate the general mobile case, in which the UAVs are assumed to move with a practical maximum velocity. Based on the previous discussion, we note that P3-2 is a non-convex problem and difficult to solve in polynomial time since it involves not only a non-convex function in the constraints but also a combinatorial sub-problem, which is a classical NP-hard problem in theory. To address these challenges, we first apply the block coordinate descent method to convert P3-2 into three sub-problems, named the grouping, resource allocation and trajectory sub-problems. In each of these sub-problems, only some of the variables are optimized, while the other variables are held fixed during the optimization process. In the following subsections, we will present the details of the algorithm for each sub-problem.

5.1. Grouping Sub-Problem

The grouping sub-problem is of critical importance to the high efficiency of the network, especially with a moderate maximum number of UAVs. Although traditional clustering algorithms such as the K-means [65] and spectral clustering algorithms can be directly employed to group devices based on their geometric information, the above methods neglect the workload imposed by the data collection process in the UAV-enabled communication scenario, which goes beyond the geometric information, and thus lead to inefficiency in this scenario. In [42,50], the authors applied the travelling salesman problem (TSP) and its variant with neighbourhoods (NTSP) to initialize the trajectory of a UAV in a multi-device scenario, in [66,67], Dubins TSP method was developed to address trajectory for Dubins vehicle, e.g.,fixed-wing UAV and in [55], the authors further extended the multiple travelling salesmen problem (MTSP) to a multi-UAV application scenario. Compared to the classical geometry-based grouping approach, a satisfactory solution to the MTSP problem can be obtained through heuristic methods such as genetic algorithms [68], and the fitness of the genetic function in such an algorithm can be adjusted to meet the requirements of practical communication scenarios.

Remark: Although genetic-based grouping algorithms are still locally optimal and time consuming in general, such algorithms have excellent parallelization characteristics; therefore, the MTSP and its variant with neighbourhoods (N-MTSP) are well suited for solving the grouping problem.

Nevertheless, in our scenario, the effects on the fitness should be considered along with the presence of interference, which leads to difficulties in traditional genetic algorithms, as only the waypoints of a trajectory are represented in the chromosome of a genetic algorithm, and the structure of the trajectory generated from these waypoints with the maximal velocity is similar to the hovering model instead of the flying model. Fortunately, the hovering model gives a stricter lower bound than the flying model with respect to the completion time [55]. To facilitate the estimation of the practical average uplink rate, we assume that the hovering point is just above each served device; this assumption should yield satisfactory accuracy when the interference distance is sufficiently large. We also assume that each UAV collects the data from its associated device at its hovering point while suffering interference transmitted from the other devices with equal visiting order numbers associated with the other UAVs.

To formulate this assumption mathematically, we use Y_n to denote the serving order number in the corresponding group $\mathcal{G}_n$, and we further define $\mathrm{Y}_n(j) = 0, j > |\mathcal{G}_n|, n \in \mathcal{N}$, to avoid ambiguity in the analysis process and set $\mathbf{w}_0 = (0, 0)$. Thus, the completion time for each UAV consists of two components, namely, the time for travelling and the time for data collection, and can be expressed as follows:

$$\hat{T}_n = \sum_{m=1}^{|\mathcal{G}_n|-1} \frac{\mathbf{w}_{\mathrm{Y}_n(m+1)} - \mathbf{w}_{\mathrm{Y}_n(m)}}{V_{\max}} + \frac{\mathbf{w}_{\mathrm{Y}_n(1)} - \mathbf{w}_I}{V_{\max}} + \frac{\mathbf{w}_F - \mathbf{w}_{\mathrm{Y}_n(|\mathcal{G}_n|)}}{V_{\max}} + \sum_{j=1}^{|\mathcal{G}_n|} \frac{D_{\mathrm{Y}_n(j)}}{\underline{R}_{n,j}} \tag{46}$$

where $\mathbf{w}_I = \mathbf{q}_n^I$, $\mathbf{w}_F = \mathbf{q}_n^F$, $\underline{R}_{n,j} = \log_2\left(1 + \frac{\frac{\beta_0 p_u}{H^2}}{\sum_{k=1,k\neq n}^{N} \frac{\Pi_{k,j}\beta_0 p_u}{\left\|\mathbf{w}_{Y_k(j)} - \mathbf{w}_{Y_n(j)}\right\|^2 + H^2} + \sigma^2}\right)$ and $\Pi_{k,j} = \begin{cases} 1, & 1 \le j \le |\mathcal{G}_k| \\ 0, & \text{otherwise} \end{cases}$.

The weighted fitness function of the genetic algorithm for the scenario with interference can be presented as follows:

$$1/\hat{f} = \mu \times \max_n \hat{T}_n + (1-\mu) \times \frac{1}{N}\sum_{n=1}^{N} \hat{T}_n \tag{47}$$

where μ denotes a weight coefficient used to strike a desired balance between the fairness of the maximal working time and the average working time.

Based on the above considerations, we apply the genetic algorithm to group the devices. Figure 3 shows the results of two initializations with 3 UAVs and 18 devices, which lead to distinct performance but the same travel distance. As a result that the interference conditions are considered in the fitness function in our proposed algorithm, the scheme shown on the right can provide better performance than that shown on the left because the maximal distances between the active devices are obtained along the trajectories.

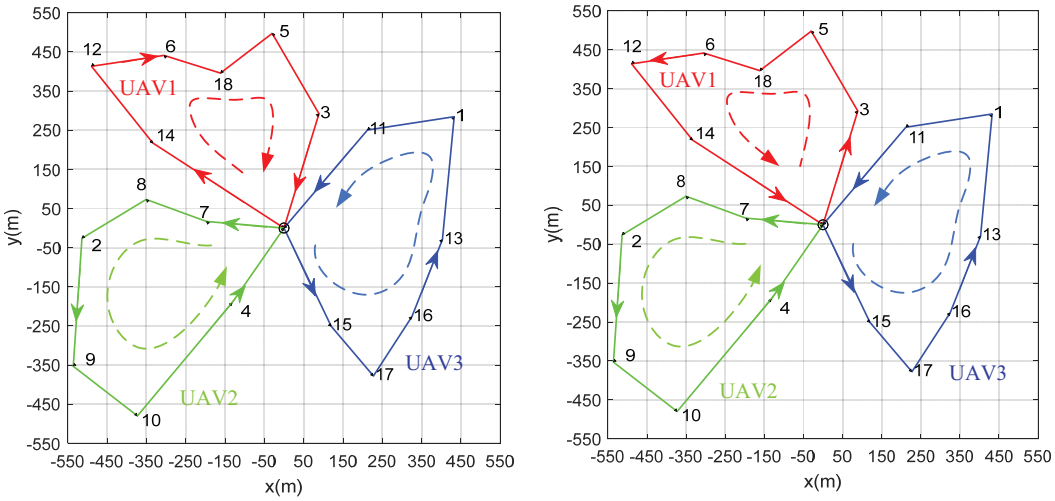

(**a**) Waypoints and ordering for scheme 1 (**b**) Waypoints and ordering for scheme 2

Figure 3. Illustration of the differences in the results of the modified genetic algorithm with two trajectory initializations: (**a**) The results with an initialization of the trajectories and visiting orders for the three UAVs in which two UAVs travel in the anticlockwise direction; (**b**) The results with another initialization of the scheme in which all UAVs travel in the anticlockwise direction.

5.2. Resource Allocation Sub-Problem

In this subsection, we aim to optimize the resource allocation to maximize the corresponding objective with given grouping and trajectory information. Based on P3-2, we can rewrite the resource allocation sub-problem as P4 below:

$$\begin{aligned} (\text{P4}): \min_{\{\mathbf{A}',\mathbf{B},\eta\}} \quad & \eta \\ s.t. \quad & (17)-(21), (27) \end{aligned} \tag{48}$$

P4 is a mixed-integer non-convex problem and is difficult to solve efficiently in general because of the binary variable constraint (19) and the upload requirements (29). To address

this intractable problem and avoid dealing with the binary variables, we attempt to exploit the underlying characteristics of the device groups to recast the above problem into a more tractable equivalent form.

Depending on the network setup, in each slot m, at most one device is associated with its scheduled UAV, which means that the devices $\bar{u} = \{\kappa | \kappa \neq u, \kappa \in \mathcal{G}_n, n = \mathcal{G}^{-1}(u)\}$ should not be associated with a UAV once the uth device has been linked with. Based on this fact, we can recast the original problem by introducing a penalty function $\psi_u[m]$ as follows:

$$(\mathrm{P4}-1): \min_{\{\mathbf{v},\boldsymbol{\psi},\eta\}} \quad \eta$$

$$s.t. \quad \sum_{m=}^{M}\sum_{n=1}^{N} v_{n,u}[m]p_u \leq E_u/\delta t, \quad \forall u \in \mathcal{U} \tag{49}$$

$$\sum_{n=1}^{N} v_{n,u}[m] \leq 1, \quad \forall n \in \mathcal{N}, \forall u \in \mathcal{U}, m \in \mathcal{M} \tag{50}$$

$$\sum_{u=1}^{U} v_{n,u}[m] \leq 1, \quad \forall n \in \mathcal{N}, \forall u \in \mathcal{U}, m \in \mathcal{M} \tag{51}$$

$$0 \leq v_{n,u}[m] \leq 1, \quad \forall n \in \mathcal{N}, \forall u \in \mathcal{U}, m \in \mathcal{M} \tag{52}$$

$$\frac{B\delta t}{D_u}\sum_{m=1}^{M}\sum_{n=1}^{N} v_{n,u}[m] \times \left\{\log_2\left(1+\frac{p_u(t)\beta_0 d_{n,u}^{-\alpha}}{\sum_{\substack{j=1\\ j\neq n}}\sum_{\omega\in\mathcal{G}_j} p_\omega v_{j,\omega}(t)\beta_0 d_{n,\omega}^{-\alpha}+\sigma^2}\right) - \eta_c \cdot \psi_u[m]\right\} \geq \eta, \quad \forall u \in \mathcal{U} \tag{53}$$

$$\psi_u[m] \geq \sum_{\substack{i\in G_n, i\neq u\\ n=\mathcal{G}^{-1}(u)}} v_{n,i}[m], \quad \forall u \in \mathcal{U}, m \in \mathcal{M} \tag{54}$$

where $v_{n,u}[m] \triangleq \alpha'_{n,u}[m] \times b'_u[m]$, η_c is a sufficiently large constant value and $\boldsymbol{\psi}$ is the set of all $\psi_u[m]$, $u \in \mathcal{U}$, $m \in \mathcal{M}$.

It is obvious that for any feasible solution to the original P4, the penalty term is equal to zero, and any solution to P4-1 that violates the binary setup of P4 will cause the objective value to deteriorate. Thus, if the penalty coefficient is moderately large, the optimal solution to P4-1 will approach a feasible solution to P4. However, the above problem P4-1 is still a non-convex problem due to the complicated form of the communication rate constraint (53). Thus, we introduce two auxiliary variables to recast P4-1 as P4-2, as follows:

$$(\mathrm{P4}-2): \min_{\{\mathrm{v},\boldsymbol{\psi},\lambda,\mathrm{I},\eta\}} \quad \eta$$

$$s.t. \quad I_{n,u}[m] \geq \sum_{\substack{j=1\\ j\neq n}}^{N}\sum_{\omega\in G_j} p_\omega v_{j,\omega}[m]\beta_0 d_{n,\omega}^{-\alpha} \tag{55}$$

$$\log_2\left(p_u\beta_0 d_{n,u}^{-\alpha} + I_{n,u}[m] + \sigma^2\right) - \log_2\left(I_{n,u}[m]+\sigma^2\right) - \eta_c\psi_u[m] \geq \lambda_{n,u}[m] \tag{56}$$

$$\frac{B\delta t}{D_u}\sum_{m=1}^{M}\sum_{n=1}^{N} v_{n,u}[m]\lambda_{n,u}[m] \geq \eta, \quad \forall u \in \mathcal{U} \tag{57}$$

$$(49)-(52), (54)$$

However, P4-2 is still a non-convex problem; fortunately, the underlying differences of convex expressions in the rate constraints in (56) and (57) can be addressed by means of the sequential convex approximation (SCA) approach [55]:

$$v_{n,u}[m]\lambda_{n,u}[m] = \frac{\underbrace{\left(v_{n,u}[m]+\lambda_{n,u}[m]\right)^2}_{convex} - \left(v_{n,u}[m]^2+\lambda_{n,u}[m]^2\right)}{2} \tag{58}$$

$$\log_2\left(p_u\beta_0 d_{n,u}^{-\alpha}+I_{n,u}[m]+\sigma^2\right) \underbrace{-\log_2\left(I_{n,u}[m]+\sigma^2\right)}_{convex} - \eta_c\psi_u[m] \geq \lambda_{n,u}[m] \tag{59}$$

The first-order Taylor expansion of a convex function can be applied to give the corresponding non-convex term a strictly lower-bound approximation; thus, we have the following constraints instead:

$$\Omega_{n,u}[m] \geq \lambda_{n,u}[m], \qquad \forall n \in \mathcal{N}, \forall u \in \mathcal{U}, m \in \mathcal{M} \tag{60}$$

$$\frac{B\delta t}{D_u}\sum_{m=1}^{M}\sum_{n=1}^{N}\Xi_{n,u}[m] \geq \eta, \qquad \forall u \in \mathcal{U} \tag{61}$$

where $\Omega_{n,u}[m]$ and $\Xi_{n,u}[m]$ are affine terms with respect to the optimization variables and are defined as

$$\begin{aligned}\Omega_{n,u}[m] \triangleq & \log_2\left(p_u\beta_0 d_{n,u}^{-\alpha}+I_{n,u}[m]+\sigma^2\right) - \log_2\left(I_{n,u}^r[m]+\sigma^2\right) \\ & - \frac{\log_2(e)}{I_{n,u}^r[m]+\sigma^2}\left\{I_{n,u}[m]-I_{n,u}^r[m]\right\} - \eta_c\psi_u[m]\end{aligned} \tag{62}$$

$$\begin{aligned}\Xi_{n,u}[m] \triangleq & -\frac{1}{2}\left(v_{n,u}^r[m]+\lambda_{n,u}^r[m]\right)^2+\left(v_{n,u}^r[m]+\lambda_{n,u}^r[m]\right)\left(v_{n,u}[m]+\lambda_{n,u}[m]\right) \\ & -\frac{1}{2}\left(v_{n,u}[m]^2+\lambda_{n,u}[m]^2\right)\end{aligned} \tag{63}$$

Finally, we obtain the optimization formulation P4-3 expressed as follows, which is a convex problem and can be solved efficiently by the CVX solver [69]. The initialization scheme for the related auxiliary variables will be detailed in the following subsection.

$$\begin{aligned}(\mathrm{P4}-3): \min_{\{v,\psi,\lambda,\mathbf{I},\eta\}} \quad & \eta \\ & (49)-(52),(54),(60),(61)\end{aligned}$$

5.3. Trajectory Sub-Problem

In this subsection, the algorithm for solving the optimal trajectory sub-problem given grouping and resource allocation information will be detailed. According to P3-2, the trajectory sub-problem can be formulated as P5 below:

$$\begin{aligned}(\mathrm{P5}): \min_{\{\mathbf{Q}',\eta\}} \quad & \eta \\ s.t. \quad & \frac{B\delta t}{D_u}\sum_{m=1}^{M}\sum_{n=1}^{N} v_{n,u}[m]\times \\ & \log_2\left(1+\frac{p_u\beta_0/\left(\left\|\mathbf{q}_n'[m]-\mathbf{w}_u\right\|^2+H^2\right)^{\frac{\alpha}{2}}}{\sum_{\substack{j=1\\ j\neq n}}^{N}\sum_{\omega\in\mathcal{G}_j}p_\omega v_{j,\omega}[m]\beta_0/\left(\left\|\mathbf{q}_n'[m]-\mathbf{w}_\omega\right\|^2+H^2\right)^{\frac{\alpha}{2}}+\sigma^2}\right) \geq \eta, \quad \forall u \in \mathcal{U} \\ & (25)-(27)\end{aligned} \tag{64}$$

The constraints related to the communication rate (64) and the minimal safe distance (25) are not convex; therefore, we introduce auxiliary variables to simplify the problem and employ the SCA approach to address these non-convex parts of the problem. Specifically, the anti-collision constraint can be expanded into affine terms as follows:

$$\left\|\mathbf{q'}_i[m]-\mathbf{q'}_j[m]\right\|^2 \geq -\left\|\mathbf{q'}^r{}_i[m]-\mathbf{q'}_j{}^r[m]\right\|^2+2\left(\mathbf{q'}_i{}^r[m]-\mathbf{q'}_j{}^r[m]\right)^T\cdot\left(\mathbf{q'}_i[m]-\mathbf{q'}_j[m]\right)\geq d_{\min}^2 \tag{65}$$

To simplify the problem with respect to the communication rate constraint, we introduce four auxiliary variables, $\theta_{n,u}[m]$, $L_{n,\omega}[m]$, $T_{n,u}[m]$ and $Z_{n,u}[m]$, as follows, to recast the original problem as P5-1 below:

$$\theta_{n,u}[m]=\sum_{\substack{j=1\\ j\neq n}}^{N}\sum_{\omega\in G_j}p_\omega v_{j,\omega}[m]\beta_0\left(L_{n,\omega}[m]+H^2\right)^{-\frac{\alpha}{2}} \tag{66}$$

$$L_{n,\omega}[m]=\left\|\mathbf{q'}_n[m]-\mathbf{w}_\omega\right\|^2 \tag{67}$$

$$T_{n,u}[m]=\theta_{n,u}[m]+p_u\beta_0/\left(z_{n,u}[m]+H^2\right)^{-\frac{\alpha}{2}} \tag{68}$$

$$Z_{n,u}[m]=\left\|\mathbf{q'}_n[m]-\mathbf{w}_u\right\|^2 \tag{69}$$

$$(\mathrm{P5}-1):\min_{\substack{\mathbf{Q'},\mathbf{T},\eta,\theta\\ \mathbf{L},\mathbf{Z}}}\quad \eta$$

$$s.t.\quad \eta\leq\frac{B\delta_t}{D_u}\sum_{m=1}^{M}\sum_{n=1}^{N}v_{n,u}[m]\{\log_2\left(T_{n,u}[m]+\sigma^2\right)\underbrace{-\log_2\left(\theta_{n,u}[m]+\sigma^2\right)}_{\text{convex}}\},\forall u\in\mathcal{U} \tag{70}$$

$$T_{n,u}[m]\leq\theta_{n,u}[m]+p_u\beta_0\underbrace{\left(L_{n,u}[m]+H^2\right)^{-\frac{\alpha}{2}}}_{\text{convex}} \tag{71}$$

$$L_{n,u}[m]\geq\left\|\mathbf{q'}_n[m]-\mathbf{w}_u\right\|^2 \tag{72}$$

$$\theta_{n,u}[m]\geq\sum_{\substack{j=1\\ j\neq n}}^{N}\sum_{\omega\in\mathcal{G}_j}p_\omega v_{j,\omega}[m]\beta_0\left(Z_{n,\omega}[m]+H^2\right)^{-\frac{\alpha}{2}} \tag{73}$$

$$Z_{n,\omega}[m]\leq\underbrace{\left\|\mathbf{q'}_n[m]-\mathbf{w}_\omega\right\|^2}_{\text{convex}} \tag{74}$$

$$-\left\|\mathbf{q'}^r{}_i[m]-\mathbf{q'}_j{}^r[m]\right\|^2+2\left(\mathbf{q'}_i{}^r[m]-\mathbf{q'}_j{}^r[m]\right)^T\cdot\left(\mathbf{q'}_i[m]-\mathbf{q'}_j[m]\right)\geq d_{\min}^2 \tag{75}$$

(26), (27)

where θ, $\mathbf{L}$, $\mathbf{T}$ and $\mathbf{Z}$ are the sets of all $\theta_{n,u}[m]$, $L_{n,\omega}[m]$, $T_{n,u}[m]$ and $Z_{n,u}[m]$, respectively.

There still exist three non-convex constraints (convex terms to the right of a less than or equal to sign) in P5-1, so we need to apply the SCA approach again; thus, we obtain the following inequalities by applying the first-order Taylor expansion at any given initial solution:

$$-\log_2\left(\theta_{n,u}[m]+\sigma^2\right)\geq-\log_2\left(\theta_{n,u}^r[m]+\sigma^2\right)-\frac{\log_2(e)}{\theta_{n,u}^r[m]+\sigma^2}\left(\theta_{n,u}[m]-\theta_{n,u}^r[m]\right) \tag{76}$$

$$\left(L_{n,u}[m]+H^2\right)^{-\frac{\alpha}{2}}\geq\left(L_{n,u}^r[m]+H^2\right)^{-\frac{\alpha}{2}}-\frac{\alpha}{2}\left(L_{n,u}^r[m]+H^2\right)^{-\frac{\alpha}{2}-1}\left(L_{n,u}[m]-L_{n,u}^r[m]\right) \tag{77}$$

$$\left\|\mathbf{q'}_n[m]-\mathbf{w}_\omega\right\|^2\geq-\left\|\mathbf{q'}_n{}^r[m]-\mathbf{w}_\omega\right\|^2+2\left(\mathbf{q'}_n{}^r[m]-\mathbf{w}_\omega\right)^T\cdot\left(\mathbf{q'}_n[m]-\mathbf{w}_\omega\right) \tag{78}$$

Plugging the above three terms into P5-1, we obtain P5-2, as shown below. P5-2 is a convex problem that can be efficiently solved by the CVX solver [69].

$$(\mathrm{P5}-2): \min_{\{\mathbf{Q}',\mathbf{T},\theta,\eta\}} \quad \eta$$

$$s.t. \quad \frac{B\delta_t}{D_u}\sum_{m=1}^{M}\sum_{n=1}^{N} v_{n,u}[m]\times \left\{\log_2\left(T_{n,u}[m]+\sigma^2\right)-\log_2\left(\theta^r_{n,u}[m]+\sigma^2\right)-\frac{\log_2(e)}{\theta^r_{n,u}[m]+\sigma^2}\left(\theta_{n,u}[m]-\theta^r_{n,u}[m]\right)\right\} \geq \eta \tag{79}$$

$$T_{n,u}[m] \leq \theta_{n,u}[m]+p_u\beta_0\times \left\{\left(L^r_{n,u}[m]+H^2\right)^{-\frac{\alpha}{2}}-\frac{\alpha}{2}\left(L^r_{n,u}[m]+H^2\right)^{-\frac{\alpha}{2}-1}\left(L_{n,u}[m]-L^r_{n,u}[m]\right)\right\} \tag{80}$$

$$[Z_{n,\omega}[m] \leq -\left\|\mathbf{q'}_n{}^r[m]-\mathbf{w}_\omega\right\|^2+2\left(\mathbf{q'}_n{}^r[m]-\mathbf{w}_\omega\right)^T\cdot\left(\mathbf{q'}_n[m]-\mathbf{w}_\omega\right) \tag{81}$$

(26), (27), (72), (73), (75)

5.4. Adaptive Initialization Scheme

In this subsection, the initialization scheme for the variables applied in P4-3 and P5-2 will be detailed. Based on the aforementioned sub-problems, an initial feasible solution for these variables should be provided before the iterative solution process begins. Moreover, the performance of the locally optimal solution to the resource allocation sub-problem is strongly related to the quality of initialization; thus, an adaptive initialization method for the resource allocation sub-problem is provided in this subsection. Here, we consider the general multi-UAV scenario, and Proposition 2 is given as follows.

Proposition 2. *When* $\Theta\left(\tilde{\mathbf{q}}'_n[i],\tilde{\alpha}'_{n,u}[i]\right)<0$, *the resource allocation matrix is initialized on the basis of the IC scheme; otherwise, it is better to initialize the resource allocation solution on the basis of the TD scheme. Here, the function* $\Theta(\mathbf{q'}_n[i],\alpha'_{n,u}[i])$ *is obtained by calculating the following expression, with* χ *denoting the number of co-working UAVs in the ith time interval:*

$$\Theta\left(\tilde{\mathbf{q}}'_n[i],\tilde{\alpha}'_{n,u}[i]\right)=\left(1+\frac{\beta_0 p_u}{\left(\check{L}^2_{n,i}+H^2\right)^{\alpha/2}\sigma^2}\right)^{1/\chi}-\frac{\left(\hat{L}^2_{n,i}+H^2\right)^{\alpha/2}}{(\chi-1)\times\left(\check{L}^2_{n,i}+H^2\right)^{\alpha/2}}-1$$

where $\check{L}_{n,i}=\|\mathbf{w}_{\chi_n[i]}-\tilde{\mathbf{q}}'^r_n[i]$, $\hat{L}_{n,i}=\min_{k\in\mathcal{N},k\neq n}\left\|\mathbf{w}_{\chi_k[i]}-\tilde{\mathbf{q}}'^r_n[i]\right\|$ *and* $\chi_n[i]=\left\{u\mid\tilde{\alpha}'_{n,u}[i]=1\right\}$.

Proof. Refer to Appendix B. □

Proposition 2 provides a principle for determining the initial resource allocation. On this basis, we first initialize the trajectories $\tilde{\mathbf{q}}^r_n[i]$, $n\in\mathcal{N}$, $\forall i\in\mathcal{F}$, based on consecutive lines generated between waypoints in accordance with the visiting order numbers obtained as proposed in Section 5.1 with the maximal velocity strategy and time intervals of length $\Delta t=N\times\delta t$. Then, we generate the initial resource allocation matrix $\tilde{\alpha}'_{n,u}[i]$ by applying the nearest distance principle and simultaneously set $\tilde{b}'_{n,u}[i]=1$, $n\in\mathcal{N}$, $\forall i\in\mathcal{F}$, where $\mathcal{F}=\{1,\cdots,F\}$ denotes the set of time intervals, with $F=\lfloor M/N\rfloor$.

Based on the above initialization process, we subsequently construct a list matrix $\mathbf{List}[i][n]$, $\forall i\in\mathcal{F}$, $n=1,\cdots N+1$, to record the mode information in the ith time interval, where $\chi=\mathbf{List}[i][N+1]$ indicates that the first χ devices $\mathbf{List}[i][j]$, $j=1,\cdots,\chi$, are co-working in the IC mode and the remaining $N-\chi$ devices $\mathbf{List}[i][j]$, $j=\chi+1,\cdots,N$, are working in the TD mode instead.

The update process is as follows. The first step is to determine the mode of device $\pi=\arg\min_{\tilde{u}}\overline{\tilde{R}}_{\tilde{u}}[i]$, which has the minimal uplink rate in the ith time interval, according

to Proposition 2, where $\overline{\bar{R}}_{\tilde{u}}[i] = \sum_{n=1}^{N} \bar{R}_{n,\tilde{u}}[i]$, $\tilde{u} \in \{\mathbf{List}[i][n], n = 1, \cdots, \chi\}$ and $\bar{R}_{n,\tilde{u}}[i]$ is defined in the proof of Proposition 2. If the resource mode of π is not changed, then the interference is sufficiently low; otherwise, the mode of π in the ith time interval is changed from the IC mode to the TD mode, and we update $\mathbf{List}[i][n]$, $\forall i \in \mathcal{F}$, $n = 1, \cdots, N+1$, and re-calculate $\bar{R}_{n,\tilde{u}}[i]$ and π until the mode of the device with the minimal rate remains unchanged. As the last step, we determine the initial resource mode in time slot δt based on the list of time intervals $\mathrm{List}[i][n]$.

If the IC scheme is applied, then we have

$$\alpha'^{r}_{n,u}[(i-1)N+j] = \begin{cases} 1, & u \in \{\mathrm{List}[i][n], n = 1, \cdots, \chi\} \\ 0, & \end{cases}, \forall i \in \mathcal{F}, j \in 1, \cdots, \chi$$

Otherwise, the TD scheme is employed, and the resource allocation solution is initialized as follows:

$$\alpha'^{r}_{n,u}[(i-1)N+j] = \begin{cases} 1, & u \in \{\mathbf{List}[i][n], n = j-\chi\}, j = n+\chi \\ 0, & \end{cases}, \forall i \in \mathcal{F}, j \in \chi+1, \cdots, N$$

Then, we initialize $b'_{n,u}[m] = 1$ and re-initialize the trajectories of the UAVs with time slot δt to obtain the initial trajectories in the time slot, $\mathbf{q}^r_n[m]$, $\forall n \in \mathcal{N}$, $\forall m \in \mathcal{M}$. The initialization of the other auxiliary variables is not difficult to obtain based on the initial resource allocation matrix and trajectory tensor. Considering space limitations, we omit the corresponding description here for brevity.

Finally, based on the above discussions, the algorithm for solving the joint adaptive resource allocation and UAV trajectory design problem (P3-2) is summarized in Algorithm 1.

Algorithm 1 Algorithm 1 for solving problem (P3-2)

Input:

The device locations $\{\mathbf{w}_u\}$, $u \in \mathcal{U}$, and all other simulation parameters listed in Table 2;
The execution time t from the 1-D search method in (28);
The grouping information $\mathcal{G}$ associated with the UAVs and the corresponding waypoints and their ordering based on the heuristic genetic scheme presented in Section 5.1.

Output:

The optimal solution to the resource allocation and UAV trajectory design problem P3-2.

1: Initialize the iteration step, $r = 0$;
2: **Repeat** the outer iteration process:
3: Given execution time t and $V_{\max}$, initialize the resource allocation and UAV trajectory solution with the
adaptive initialization scheme presented in Section 5.4;
4: Initialize the auxiliary variables $I^r_{n,u}[m]$ and $\lambda^r_{n,u}[m]$;
5: Given the initial groups $\mathcal{G}_n$, $n \in \mathcal{N}$, the initial resource allocation matrix $v^{(r)}_{n,u}[m]$, and the initial trajectory
of each UAV, $\mathbf{q}'^{(r)}_n[m]$, $n \in \mathcal{N}$, $m \in \mathcal{M}$, find the optimal resource allocation scheme $v^{(r+1)}_{n,u}[m]$ by iteratively
solving problem P4-3 iteratively;
6: Update the auxiliary variables $\theta^r_{n,u}[m]$ and $L^r_{n,u}[m]$;
7: With the obtained groups $\mathcal{G}_n$, $n \in \mathcal{N}$, and the optimal resource allocation scheme $\boldsymbol{v}^{(r+1)}_{n,u}[m]$, find the
optimal UAV trajectories $\mathbf{q}'^{(r+1)}_n[m]$ by iteratively solving sub-problem P5-2;
8: Set $r = r + 1$;
9: **Until** the solution converges to a given accuracy ε or the maximum number of iterations is reached.

6. Numerical Results

In this section, numerical results are presented to illustrate the characteristics of the proposed joint adaptive interference management and trajectory design algorithm and verify its effectiveness.

We consider a wireless UAV-enabled data collection scenario in which all UAVs share the same constant altitude, which is set to $H = 100$ m to satisfy the minimal height requirement. Moreover, the maximum speed of a drone is set to $V_{\max} = 25$ m/s, similar to that of a practical commercial drone [70]; during task execution, each UAV can adjust its velocity between zero and this maximum speed to meet the requirements of the trajectory design. The total bandwidth of the system is set to 3 MHz, which is shared among all devices, and the transmit power of each ground device is assumed to have a constant value of 0.05 W (17 dBm).

In this scenario, we mainly focus on the case of sensors distributed in the natural environment to monitor changes in a river to avoid disasters, as in classical flood management applications. The data to be uploaded include not only text information but also images from optical sensors; thus, the data size is much larger than for traditional IoT devices. On the other hand, the data size is also related to the duration of the collection period and depends on the specific application scenario. We set the data upload requirement for each device to 120 Mb for simplicity.

Finally, the channel power at a reference distance of 1 m is -60 dB. The simulation parameters are as listed in Table 2 unless otherwise stated.

Table 2. Simulation parameters for the multi-UAV-enabled data collection network.

Parameters	Explanation	Values
H	Height of the UAVs	100 m
B	Bandwidth of the network	3 MHz
α	Path loss exponent	2.0
$V_{\max}$	Maximum speed of a UAV	25 m/s
σ^2	Noise density at the receiver	-105 dBm *Remark*: $(\sigma^2 = -110 + \log_2(B) \times 3)$
β_0	Receive power at a reference distance of 1 m	-60 dB
p_u	Transmit power of a ground device	0.05 W (17 dBm)
δt	Duration of a time slot	0.5 s ($V_{\max}\delta t = 10 \ll H = 100$)
D_u	Total size of data to be uploaded	120 Mb
$d_{\min}$	Minimum safe distance between any two UAVs	5 m
ε	Tolerance of iterative optimization	ε=10^{-3}

6.1. Results for the Joint Problem in the Basic Network Scenario

In this subsection, we first consider the basic network scenario with two UAVs ($N = 2$) and four symmetrically distributed ground devices ($U = 4$) to validate the performance of our proposed algorithm, and we set the maximum UAV speed sufficiently high that the maximal speed constraint (26) in P3-2 can be eliminated.

In the first case, we consider four devices numbered from 1 to 4, located at $(\pm 40, 0)$ and $(\pm 20, 0)$, and in the second case, we consider another four devices numbered from 5 to 8, located at $(\pm 300, 0)$ and $(\pm 200, 0)$; moreover, we set the UAVs' initial and final locations to be the same, at $(0, -100)$. To obtain an insightful solution to (P3-2), in this scenario, we set the duration to 26 s in each case and initialize our simulation using the algorithm presented in Section 5.4.

Figure 4 shows the convergence of the algorithm with different initialization schemes. It is observed that in case 1, because any two devices are in close proximity to each other, serious interference occurs, and the network prefers to adopt the TD scheme to manage this interference. Our proposed adaptive initialization scheme is therefore equivalent to the TD initialization scheme, and hence, relatively stable, convergent performance is obtained with the proposed scheme. In contrast, an unsatisfactory solution is obtained when IC

initialization is employed, resulting in only a quarter of the throughput obtained with our proposed method because the solution is affected by the quality of the initialization and converges to a local optimum. In contrast, in case 2, the distance between any two devices is sufficiently large to attenuate the interference, and the IC initialization scheme is preferable to improve the system performance; thus, our adaptive initialization scheme is equivalent to the IC initialization scheme, and the resulting throughput performance is superior to that achieved with the TD initialization scheme by 22%. As a result that the rate for the IC mode is related only to the distance between the devices, within a few iterations of the resource allocation process, the common throughput of the network rapidly converges, with more time slots being allocated to devices that are subjected to stronger interference. The above results validate our analysis in Section 4 and the effectiveness of the adaptive initialization scheme.

The optimal horizontal trajectories of the UAVs for the two cases are presented in Figure 5. Here, the analytical optimal hovering points in the IC scheme for two UAVs and two devices are used as the benchmark [59]. It is observed that the optimal displacements of the UAVs for case 2 perfectly agree with the theoretical optimal hovering displacements, thus validating the correctness of the proposed algorithm. In addition, the hovering points of the two UAVs for case 1 are just above their corresponding served devices, as the TD scheme is employed to avoid serious interference and thereby enhance the system throughput performance. In case 2, the two UAVs fly to their optimal hovering points under the IC scheme, which are slightly offset from the locations of the corresponding devices to strike a balance between the optimal displacements with respect to the served devices for data harvesting and the interference caused by the presence of another active device. Additionally, as proven in the previous section, it is observed that as the distance between the two devices increases, the optimal hovering locations of the UAVs for the IC scheme approach their corresponding served devices.

When the devices are adjacent (i.e., the stage 1 region, as depicted in Figure 6), the interference for data collection is strong enough that the proposed adaptive interference management approach will adaptively select the TD scheme to control the interference, making the proposed scheme equivalent to the TD scheme; in this regime, the common throughput is higher by at least 30% than that achieved with the IC scheme. With increasing distance between the devices (i.e., the stage 2 region, as depicted in Figure 6), the outer pair of devices switches from the TD mode to the IC mode, while the inner pair of devices remains in the TD mode. To enhance the common throughput of the network, the system allocates more resources to the inner pair of devices; consequently, the common throughput is increased by up to 10% compared to that achieved under either the TD or IC scheme alone. Meanwhile, it can be observed from the curve that the slope of the common throughput for the adaptive method decreases with increasing f_d, indicating that the derivative of the rate for the IC mode satisfies $\frac{\partial R^{IC}(L)}{\partial L} < 0$, in agreement with our proof of Proposition 1. When the distance between the devices is sufficiently large (i.e., the stage 3 region, as shown in Figure 6), all devices are served with the IC scheme, and thus, the proposed method is equivalent to the IC method; in this regime, the common throughput of the system is increased by at least 12% compared to that achieved in the TD mode.

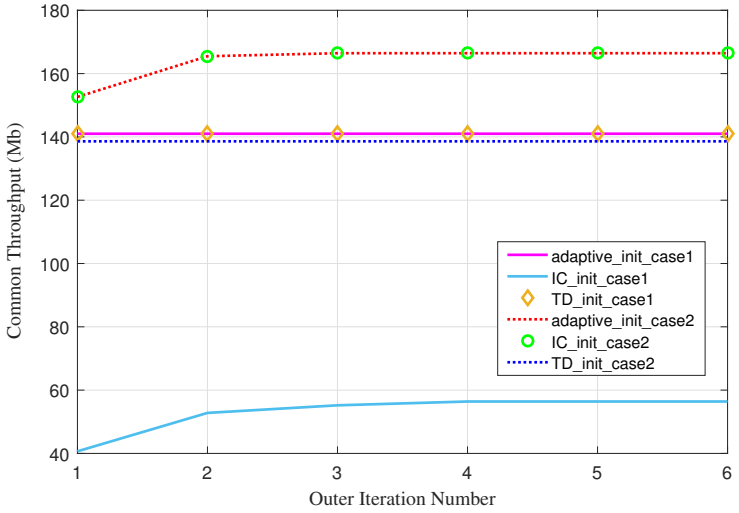

Figure 4. Convergence of the proposed algorithm in different cases.

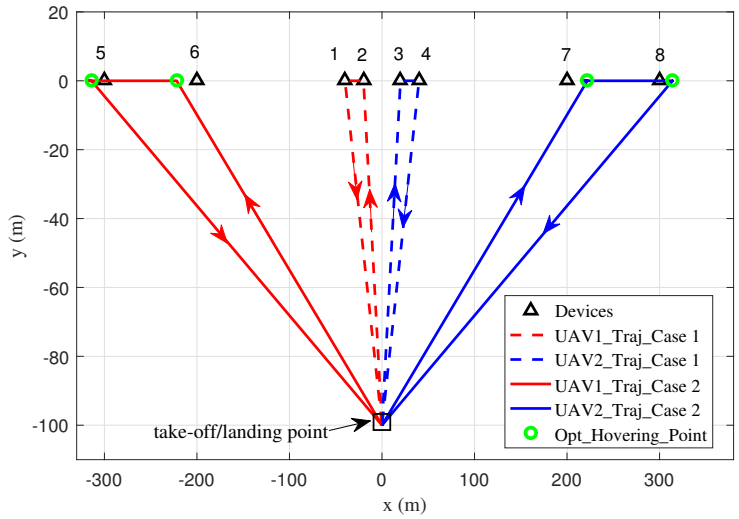

Figure 5. Optimal trajectories of the two UAVs for the quasi-stationary scenario with $T = 26$ s.

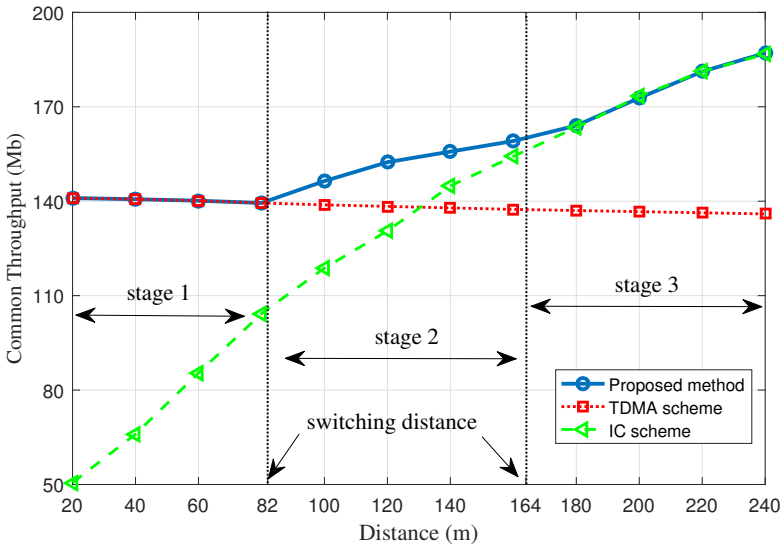

Figure 6. Common throughput of the network versus the distance between devices for different schemes.

The above experimental results validate the adaptive nature of the proposed algorithm and indicate that the proposed method endows the network with more flexibility, thus enhancing the common throughput relative to what can be achieved by employing either the IC or TD resource scheme alone. To further quantitatively evaluate the resource allocation performance and draw insightful conclusions, we introduce a metric $\Gamma = \sum_{n=1}^{N}\sum_{u=1}^{U}\sum_{m=1}^{M} \alpha'_{n,u}[m]/(N \times M)$ to differentiate the performance of the IC and TD modes with respect to resource allocation. From the above definition, it is clear that this metric is upper bounded by 1, and we have $\Gamma_{\mathrm{IC}} = 1$ and $\Gamma_{\mathrm{TDMA}} = 1/N$. According to the above experimental results, the value of this metric approaches 1 with slight interference and decreases with severe interference. In the next subsection, we will present further discussion based on the experimental results for the general scenario.

6.2. Results for the General Mobile Scenario

In this subsection, we evaluate the performance of our proposed solution in a scenario involving 3 UAVs with a finite maximum velocity (25 m/s) and 18 ground devices uniformly distributed over a $[-550, 550] \times [-550, 550]$ area. The maximal energy consumption of each device is set to 1.0 J. The initial and final locations of all UAVs are set to $(0, 0)$ for simplicity. To validate the effectiveness of the proposed method, dynamic frequency-division multiple access (FDMA) schemes based on the hovering mode (Hmode) and the flying mode (Fmode) are introduced as benchmarks [55]. Specifically, the bandwidth of each UAV in the above two FDMA schemes is 1 MHz, and the noise density σ_0 is taken to be -110 dBm for fair comparison. The convergence results of the proposed algorithm are plotted relative to the left axis in Figure 7 to validate its convergence behaviour.

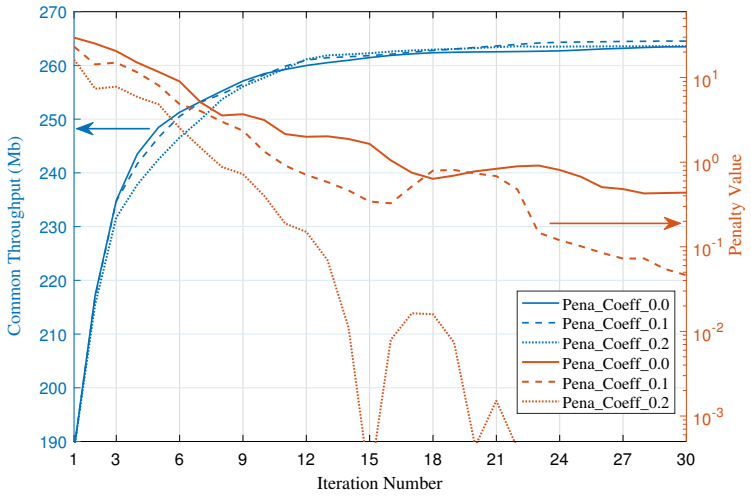

Figure 7. Convergence results of the proposed algorithm with different penalty coefficients.

Moreover, to validate the effectiveness of the resource allocation algorithm, we consider the following penalty value:

$$f_{pena} = \sum_{m}^{M}\sum_{u}^{U}\sum_{n}^{N} v^*_{n,u}[m]\psi^*_u[m]$$

From the data plotted against the right axis in Figure 7, it can be observed that with a small penalty term in the formulation, the optimal solution to P4-1 converges to a feasible solution to P4, indicating that these problem formulations are equivalent at the optimal point and thus validating our algorithm. In contrast, when $\eta_c = 0$, the optimal solution to P4-1 is merely a relaxed solution to the original optimization problem P4, and the equivalence does not always hold. Moreover, the penalty value fluctuates during the iterative process and finally converges because the SCA approach is applied to the resource

allocation sub-problem, and the optimal solution is iteratively obtained to strike a balance between the objective and penalty values.

In this scenario, the minimal completion times for the Hmode scheme, the Fmode scheme and our proposed scheme are 137 s, 86 s and 74 s, respectively, indicating that the proposed adaptive interference management scheme outperforms the benchmarks. According to the energy consumption model for a rotor-wing UAV [45,48], the aerodynamic power consumption of each vehicle in each time slot can be expressed as

$$P_{\mathrm{UAV}}[n] = P_{\mathrm{level}}[n] + P_{\mathrm{drag}}[n] = \frac{\varrho_1}{\sqrt{\|\mathbf{v}\|^2 + \sqrt{\|\mathbf{v}\|^4 + 4V_{\mathrm{h}}^4}}} + \varrho_2 \|\mathbf{v}\|^3 \tag{82}$$

where ϱ_1, ϱ_2 and V_h are constant parameters related to the UAV mechanics and aerodynamics; in this paper, the above three parameters are the same as in [48]. Based on the above energy model, the maximal aerodynamic consumption values of each UAV under the different schemes are 43 kJ, 15.6 kJ and 12.9 kJ, respectively. The energy consumption under the Hmode scheme is more than twice that under the other two schemes, as a UAV in the hovering state ($v = 0$) consumes more energy than a UAV in the flying state to overcome aerodynamic effects and keep its body static in the sky; thus, the Hmode scheme yields the worst performance.

Furthermore, Figure 8 shows the UAVs' optimal horizontal trajectories under the different schemes. Here, only the waypoints for the Hmode scheme are presented to preserve the clarity of the figure. There are obvious differences between the Hmode trajectories and those under the other two schemes, with the collection points of the Hmode trajectories being rather far away from the served devices, leading to lower efficiency and unsatisfactory communication quality. In contrast, only slight differences exist between the trajectories found using our method and the Fmode scheme. As shown in the enlarged partial views in Figure 8, the optimal hovering points of the adaptive method are different from those of the orthogonal scheme, reflecting how the IC scheme is applied to enhance the common throughput at times when the interference is sufficiently low.

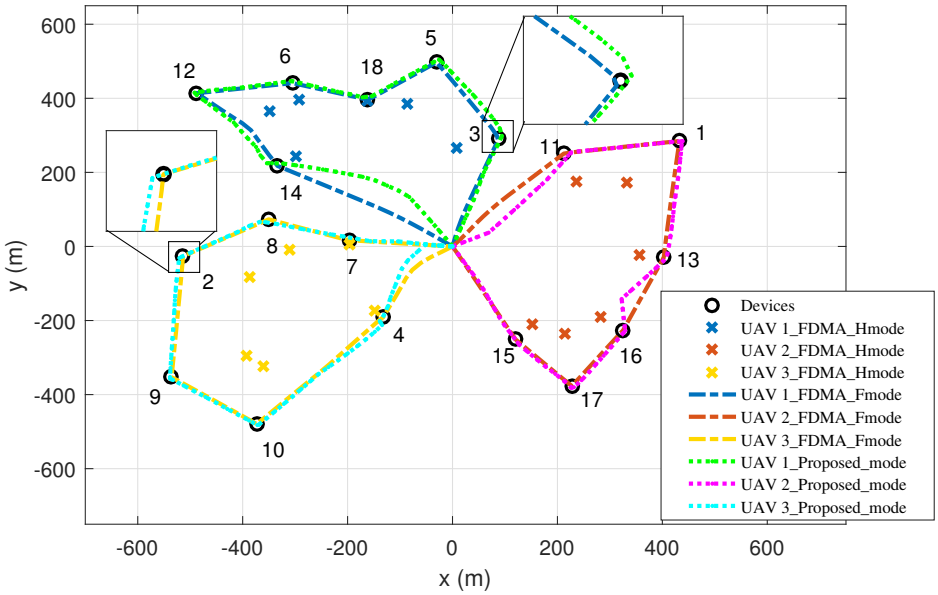

Figure 8. The optimal trajectories of multiple UAVs under different schemes.

Figure 9 presents the optimal resource allocation solution for each of the 3 UAVs, from which it can be observed that only a small number of time slots are optimized to use the TD scheme (i.e., the initial 3 time slots and final 3 time slots, as shown in the top and bottom panels, respectively). In most of the other time slots, the system is operating in

the IC mode or at least in the hybrid mode, and we obtain $\Gamma_{\text{mobile}} = 0.83$ for this scenario, which approaches the theoretical bound; thus, it is reasoned that better performance can be obtained.

Finally, in this subsection, we present the completion time results obtained with the different algorithms when the network is subject to different path loss exponents. Although free-space channel conditions are mostly assumed in UAV-enabled communication scenarios due to the highly flexible deployment of the vehicles, the path loss exponent α may vary in different practical environments. Therefore, the performance in terms of the minimal completion problem with different path loss exponent settings deserves investigation.

The simulation results are presented in Figure 10. It is observed that the completion time under both the Hmode and Fmode schemes grows significantly with an increasing path loss exponent, as the achievable rate of the system with orthogonal channels depends only on the SNR, which decreases exponentially with increasing α. Specifically, with each increment of 0.1 in α from 2.0 to 2.4, an extra 10 s is needed to complete the data collection mission, and the completion time increases exponentially when α is larger than 2.4. In contrast, for our proposed adaptive algorithm, the achievable rate with the IC scheme is related to the SINR, which is relatively insensitive to the change in α because the interference, which affects the achievable rate more strongly than the noise does, simultaneously decreases with increasing α; thus, a relatively stable completion time result can be obtained when the reference receive power is sufficiently large. For example, when $\beta_0 = -60$ dB, our proposed algorithm achieves a stable completion time (fluctuating around approximately 73 s with a variance of 1 s) as the exponential path loss varies from 2.0 to 2.2, and similar stable behaviour of the completion time (fluctuating around approximately 61 s with a variance of 2 s) extends up to $\alpha = 2.5$ when $\beta_0 = -55$ dB.

The above simulation results reveal that the proposed algorithm exhibits better robustness than the benchmark methods with solely orthogonal channels. Robustness is of critical concern in the minimal completion optimization problem, although it has always been overlooked in the previous literature.

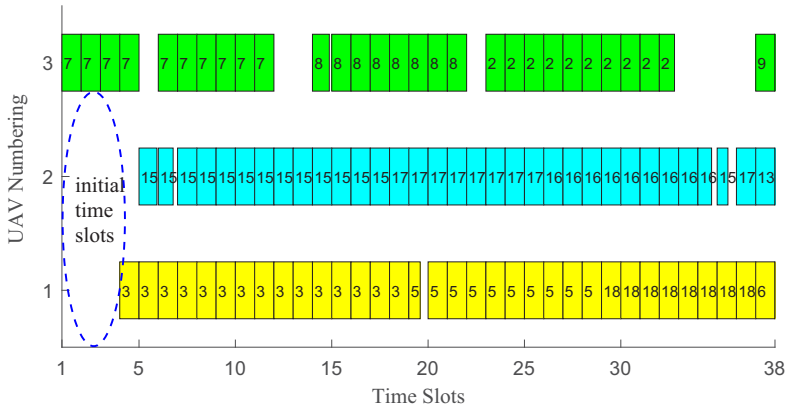

(**a**) Resource allocation over the first interval

Figure 9. *Cont.*

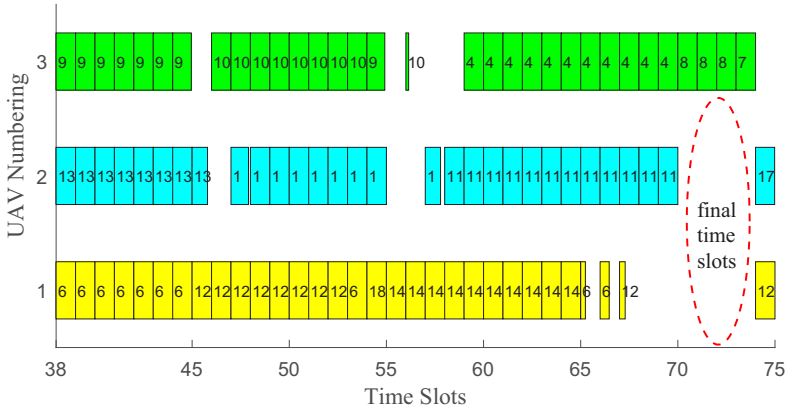

(**b**) Resource allocation over the second interval

Figure 9. Optimal resource allocation over different time slots for multiple UAVs in the general scenario: (**a**) The optimal resource allocation over the time slots in the first half of the total duration; (**b**) the optimal resource allocation over the time slots in the second half of the total duration.

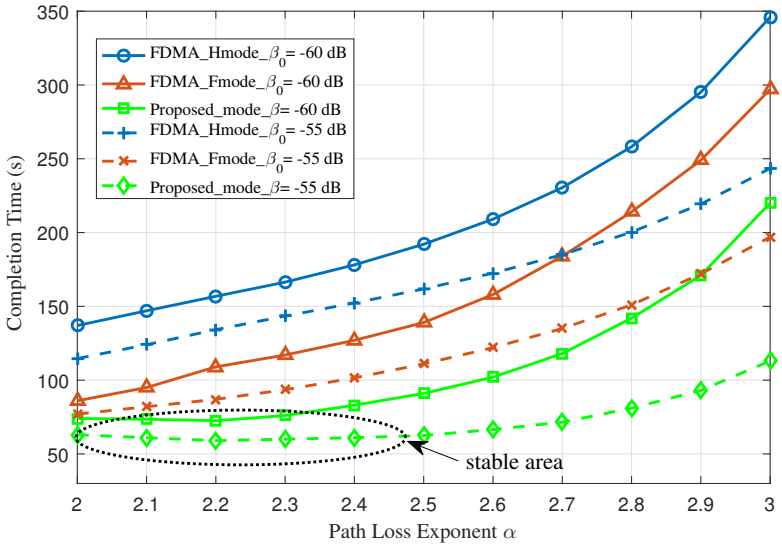

Figure 10. The completion time for network data collection versus the path loss exponent under different schemes.

6.3. Effects of the Maximum Number of UAVs on The Network

In this subsection, we will investigate the effects of the maximal number of UAV on the completion time for the network with different schemes, and then give a basic principle to deploy the UAV in complicated scenario based on a metric.

Many studies have discussed ways to enhance system performance by taking advantage of multiple UAVs under various network structures and frameworks [21,31,55,57]; however, the algorithms proposed in these studies have inherent limitations and can only adapt to a certain number of UAVs. Unfortunately, there is insufficient research on this subject. To compare different frameworks and investigate this problem, we take the CoMP scheme with multiple UAVs as a benchmark approach [38]. In this section, we consider a new scenario involving 4 UAVs and 24 devices uniformly distributed over a $[-800, 800] \times [-800, 800]$ area, where the bandwidth of the network system is set to 4 MHz. Figure 11 shows the completion time of the system versus different numbers of UAVs. It is observed that the Fmode scheme offers almost equal performance to our proposed algorithm when a single UAV is employed, as they are equivalent to each other in the single-UAV case for this scenario, and both achieve superior performance compared to the Hmode scheme, reducing the completion time by approximately half. In contrast,

the CoMP approach is not suitable for single-UAV deployment because of the inherent structure of this framework.

When two UAVs are deployed in the network, our proposed algorithm shows the best performance, with the slope of the corresponding curve being greater than those for the other two schemes; this is because the IC scheme is adaptively applied in our method, achieving an additional communication rate gain in the network by coordinating the interference. Meanwhile, for the CoMP approach, because the number of UAVs is limited, the gain achieved through beamforming is relatively low; thus, this method shows the worst performance.

Furthermore, as the number of UAVs increases, our proposed algorithm still outperforms the benchmarks when four UAVs are deployed in this scenario. Interestingly, the Hmode scheme yields a better curve slope than the Fmode scheme or our proposed scheme because the UAVs harvest data only while hovering at the optimal points, and thus, the completion time for the Hmode scheme consists of two separate components: the time for travelling and the time for data collection. Hence, with an increase in the number of UAVs, the system gain arises from both of these components. In contrast, in the Fmode scheme, the UAVs collect data while flying, and thus, the performance gain comes only from the reduction of the distance; thus, the performance gain is less than that of the Hmode scheme. Moreover, the slope of the curve corresponding to our proposed method is also greater than that for the Fmode scheme, as an additional rate gain is achieved through adaptive interference management and trajectory design, as expected. It is also interesting to observe that the CoMP method shows the advantages of the virtual beamforming effect and exhibits the maximal curve slope when four UAVs are deployed, as the number of virtual antennas is equal to the number of UAVs, and thus, more gain can be achieved through the deployment of more vehicles. We can see that the completion time with our proposed method is at least 25% less than those achieved with other dynamic orthogonal benchmark schemes when 4 UAVs are deployed.

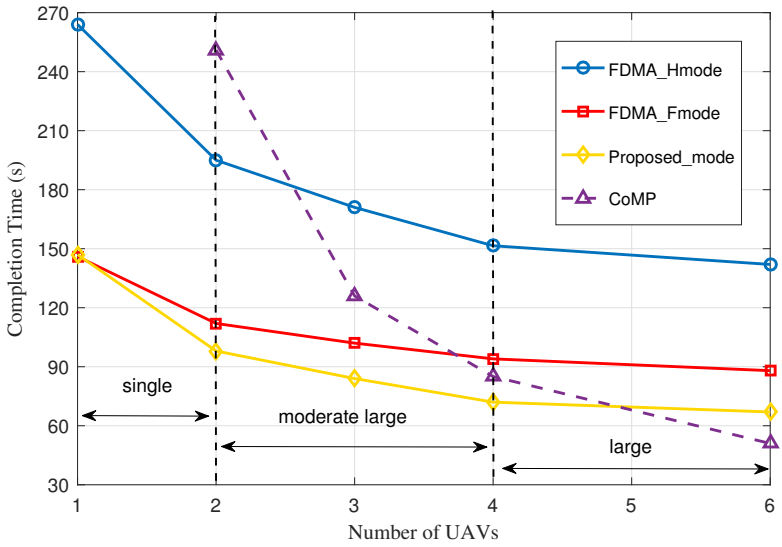

Figure 11. The completion time versus the number of UAVs under different schemes.

When 6 UAVs are deployed, the performance of the different schemes changes significantly. In particular, the slopes of the curves for both the Hmode and Fmode schemes are nearly zero, indicating that the average frequency resources allocated to each UAV are insufficient to harvest the data in a timely manner and that these orthogonal schemes tend to be inefficient with a large number of UAVs. Moreover, for our proposed algorithm, the completion time in the 6-UAV case is unfortunately only 5 seconds less than that in the 4-UAV case; this is because as the number of UAVs increases, the interference introduced by the additional active devices is strongly multiplied, driving more UAVs to employ the

more conservative resource allocation scheme (i.e., the TD scheme) over more time slots to maintain the system throughput, resulting in a loss of system gain. In contrast, with more severe interference, the efficiency of the CoMP architecture remains very high because the CoMP framework takes advantage of multi-device interference to cooperatively enhance the system performance, allowing this framework to effectively adapt to the deployment of a large UAV swarm.

The adaptability of our proposed algorithm depends on the scale of the system, the number of UAVs, the distribution of the devices and the network setup; hence, it is difficult to give an analytical principle in general. Therefore, in the last part of this subsection, we will attempt to identify the key factor that exerts the most substantial effect on the performance of the system under the proposed algorithm. To answer this question, the completion times with different numbers of UAVs and the corresponding resource metric values are shown in Figure 12. As observed, the completion time decreases dramatically when the resource metric value is greater than 0.8, and as the resource metric value decreases, the slope of the completion time curve also decreases and may even become zero. Specifically, the completion time curve tends to flatten when the metric value is below 0.6, thus leading to lower system efficiency with a large number of UAVs. This indicates that the resource metric value of the proposed algorithm is correlated with the slope of the completion time curve, and thus, it can be regarded as a criterion for evaluating the maximum number of UAVs that can be effectively deployed.

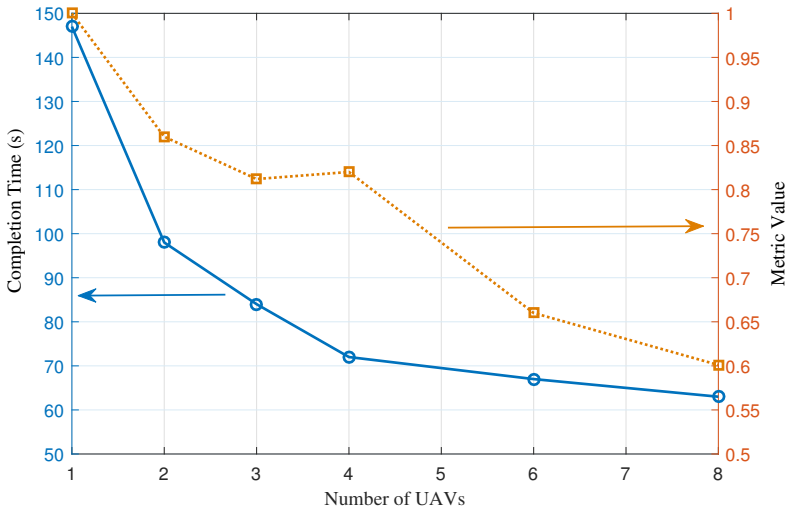

Figure 12. The relationship between the network efficiency and the resource metric value in the multi-UAV scenario.

7. Conclusions

This paper studies the optimization of the minimal completion time for a data collection scenario with multiple UAVs, in which a set of ground devices upload data to their corresponding scheduled UAVs. We combine the advantages of both the time-division and interference coordination schemes and provide a general formulation for the multi-UAV scenario that not only is compatible with both modes but also allows adaptive adjustment to an optimal resource allocation scheme and trajectory design solution to enhance the network performance when faced with a complicated interference environment. We propose an efficient algorithm to solve the non-convex problem formulation and obtain a satisfactory solution. It is shown via experiments that the completion time achieved with our proposed algorithm with joint grouping, resource allocation and trajectory optimization is at least 25% less than those achieved with other dynamic orthogonal benchmark schemes when 4 UAVs are deployed. Finally, we present a quantitative metric and a corresponding principle concerning the applicability of the proposed algorithm, which can facilitate the

development of a strategy for determining the maximum number of UAVs to be employed in practice.

Author Contributions: Conceptualization, W.P.; methodology, W.P.; software, W.P.; validation, W.P.; writing—original draft preparation, W.P.; writing—review and editing, W.P.; supervision, J.Z.; project administration, J.Z.; funding acquisition, W.P. All authors have read and approved the published version of the manuscript.

Funding: This research was funded by the National Natural Science Foundation of China under Grant 61771047 and in part by the China Scholarship Council.

Conflicts of Interest: The authors declare no conflict of interest. The funders had no role in the design of the study; in the collection, analysis or interpretation of data; in the writing of the manuscript; or in the decision to publish the results.

Appendix A. Proof of Proposition 1

The proof consists of five parts,

- For case 1, according to Lemma 2, the system will take the TD scheme over the total completion time since the interference is strong enough. We also notice that the optimal resource allocation solution to the network is not unique, however, the total resource allocation over time is determined if irrespective of the exact allocation at each particular time instant. Thus, we have $T_1^* = \frac{4D_u}{B\log_2\left(1+\frac{\beta_0 p_u}{H^2\sigma^2}\right)}$. As the TD scheme is adopted to allocate resources, the total completion time consists of four intervals with equal duration $T_1^*/4$, and during any of them, only one device is permitted to access to the network and the optimal hovering placement of UAV is just above on each device as the TD scheme is adopted.
- For case 2, according to Lemma 2, the system will take the different schemes over the total completion time, since the different interference experience. There are two candidate access schemes: in the first scheme, UAV1 is scheduled to device 2, while UAV2 is scheduled to device 3 at first interval and then UAV1 is scheduled to device 1, while UAV2 is scheduled to device 4 in the following interval; and in the second scheme, UAV1 is scheduled to device 1, while UAV2 scheduled to device 3 at first interval and UAV1 is scheduled to device 2, while UAV2 is scheduled to device 3 in the successive interval. As the inequality $L_2 + L_1 < L^\dagger$ is satisfied, the first access is better than the second one based on Lemma 2, therefore, the optimal resource allocation scheme is UAV1 scheduled to device 2, while UAV2 scheduled to device 3 with TD scheme each with time $T_{21} = \frac{D_u}{B\log_2\left(1+\frac{\beta_0 p_u}{H^2\sigma^2}\right)}$. In the following time interval, the system will take IC scheme, that means UAV1 is scheduled to device 1 and UAV2 is scheduled to device 4 simultaneously, as the symmetric structure it shares, the left working time is $T_{22} = \frac{D_u}{B\log_2\left(1+\frac{\beta_0 p_u/\left(\left(x_1^*-L_2\right)^2+H^2\right)}{\beta_0 p_u/\left(\left(x_1^*+L_2\right)^2+H^2\right)+\sigma^2}\right)}$, and according to Lemma 1 $x_1^* \simeq \sqrt{L_2^2+H^2}$.
- For case 3, different from case 2, as the inequality $L_2 + L_1 \geq L^\dagger$ satisfies, the optimal resource allocation should be detailed. To pick up the optimal solution, we introduce L'' and assumed that when the inequality $2L_2 \geq L''$ holds, the $2T_1 = T_2 + T_3$ holds, then we have following equation,

$$\frac{2}{R_1}=\frac{1}{R_2}+\frac{1}{R_3} \Rightarrow R_1=\frac{2R_2R_3}{R_2+R_3}=2R_2\left(1-\frac{R_2}{R_2+R_3}\right) \tag{A1}$$

where $R_1 = \log_2\left(1+\frac{\frac{\beta_0 p_u}{\left(\tilde{x}_2^*-(L_1+L_2)/2\right)^2+H^2}}{\frac{\beta_0 p_u}{\left(\tilde{x}_2^*+(L_1+L_2)/2\right)^2+H^2}+\sigma^2}\right)$ indicates the rate of IC mode for serving devices 1 and 3 simultaneously; $R_2 = \frac{1}{2}\log_2\left(1+\frac{\beta_0 p_u}{H_2\sigma^2}\right)$ indicates the rate of TD for serving devices 2 and 3; while

$R_3 = \log_2\left(1+\frac{\frac{\beta_0 p_u}{\left(\tilde{x}_3^*-L_2\right)^2+H^2}}{\frac{\beta_0 p_u}{\left(\tilde{x}_3^*+L_2\right)^2+H^2}+\sigma^2}\right)$, which indicates the rate of IC mode for serving devices 1 and 4 simultaneously, and according to Lemma 1, we have $\tilde{x}_2^* \simeq \sqrt{(L_1+L_2)^2/4+H^2}$ and $\tilde{x}_3^* \simeq \sqrt{L_2^2+H^2}$.

Without loss of generality, we fix the length of L_1, and denote $\tilde{l}, \tilde{l} \in (L_1, L_2]$ as the distance satisfies $L_1+\tilde{l} = L^\dagger$, then taking the limit of the function, we have following inequality, as $2L_2 \geq 2\tilde{l} > L^\dagger$ satisfies

$$\lim_{L_2\to\tilde{l}^+}\left\{R_1-2R_2\left(1-\frac{R_2}{R_2+R_3}\right)\right\} = R_2-2R_2\left(1-\frac{R_2}{R_2+R_3}\right)=R_2\frac{R_2-R_3}{R_2+R_3}<0 \quad \text{(A2)}$$

Thus, as the continuity of function, there must exist at least one solution which satisfies $\frac{2}{R_1} = \frac{1}{R_2}+\frac{1}{R_3}$, and in the following part, we will prove that the function $f(L) \triangleq \frac{\partial R^{IC}(L)}{\partial L}$ is strictly non-increasing with respect to L under the high SNR/INR assumption.

To prove this proposition, we first give the derivatives of the function as follows,

$$\begin{aligned} f(L) \triangleq \frac{\partial R^{IC}(L)}{\partial L} &= 2\times\log_2(e)\left\{\frac{L}{4H^2+L^2}+\frac{(x^*-L/2)\times(1/2-L/4x^*)}{(x^*-L/2)^2+H^2}\right\} \\ &= 2\times\log_2(e)\left\{\frac{1}{\frac{4H^2}{L}+L}+\frac{1/2-L/4x^*}{(x^*-L/2)+\frac{H^2}{(x^*-L/2)}}\right\} \end{aligned} \quad \text{(A3)}$$

It is noticed that $\frac{1}{\frac{4H^2}{L}+L}$ is strictly decreasing when $L > 2H$, $-\frac{L}{x^*} = -\frac{1}{\sqrt{\frac{1}{4}+\left(\frac{H}{L}\right)^2}}$ is a decreasing function with respect to L and $(x^*-L/2)+\frac{H^2}{(x^*-L/2)}$ is increasing with respect to L as $x^*-L/2 = \frac{H^2}{\sqrt{\left(\frac{L}{2}\right)^2+H^2}+\frac{L}{2}}$ is a decreasing function and $x^*-L/2 < H$. Thus, it is observed that $f(L)$ is a decreasing function with respect to L. In the following, we will exploit the above property to derive our conclusion, and firstly, for any fixed L_1, we further denote the function $J(L_2)$ as $J(L_2) \triangleq \frac{2}{R_1(L_2)}-\frac{1}{R_2}-\frac{1}{R_3(L_2)} \Rightarrow \frac{\partial J(L_2)}{\partial L_2} = \frac{R_3'(L_2)}{R_3^2(L_2)}-\frac{2R_1'(L_2)}{R_1^2(L_2)}$ and according to the aforementioned property and Lemma 2, we could see that $\frac{\partial J(L_2)}{\partial L_2} \leq 0$ with the assumption of high SNR/INR. That means $J(L_2)$ is strictly decreasing with respect to L_2. Therefore, we denote L'' as the distance makes the equation $\frac{2}{R_1}=\frac{1}{R_2}+\frac{1}{R_3}$ hold and specific value of L'' could be obtained by the 1-D bisearch method efficiently. Based on above derivation, for case 3, as the $2L_2 < L''$ condition is satisfied, the optimal resource allocation and optimal hovering displacement satisfy the rules the same as case 2.

- For case 4, the analysis process is the same as case 3, as the $2L_2 > L''$ is satisfied, the system employs the IC scheme to complete the task during the total duration and within the first interval $\left(0, T_{41}^*\right]$, UAV 1 will hover at $\left(-x_4^*, 0\right)$ and associates with device 1, meanwhile, UAV 2 hovers at $\left(x_3^*, 0\right)$ and pairs with device 3; and within the second time interval $\left(T_{41}^*, 2T_{41}^*\right]$, UAV 1 hovers at $\left(-x_3^*, 0\right)$ and associates with device 2, meanwhile UAV 2 hovers at $\left(x_4^*, 0\right)$ and pairs with device 4. According to

Lemma 1, the optimal hovering displacements are $x_3^* \simeq \sqrt{(L_1+L_2)^2/4+H^2} - \frac{L_2-L_1}{2}$ and $x_4^* \simeq \sqrt{(L_1+L_2)^2/4+H^2}+\frac{L_2-L_1}{2}$, where

$$T_{41}^* = \frac{D_u}{B\log_2\left(1+\frac{\beta_0 p_u/\left(\left(x_3^*-x_2\right)^2+H^2\right)}{\beta_0 p_u/\left(\left(x_3^*+x_1\right)^2+H^2\right)+\sigma^2}\right)} \tag{A4}$$

- For case 5, as the interference is slight enough, the system takes IC mode over the total time slots, as the same analysis mentioned above, there exist two allocation schemes, one is during the first interval $\left(0, T_{61}\right]$, UAV 1 associates with device 1 and collects data at $[-x_2^*, 0]$, and simultaneously, UAV 2 associates with device 3 and harvests at $[x_2^*, 0]$; where $T_{61} = \frac{D_u}{B\log_2\left(1+\frac{\beta_0 p_u/\left(\left(x_2^*-L_1\right)^2+H^2\right)}{\beta_0 p_u/\left(\left(x_2^*+L_1\right)^2+H^2\right)+\sigma^2}\right)}$ and $x_2^* \simeq \sqrt{L_1^2+H^2}$; and in the second interval $T_{62} = \frac{D_u}{B\log_2\left(1+\frac{\beta_0 p_u/\left(\left(x_1^*-L_2\right)^2+H^2\right)}{\beta_0 p_u/\left(\left(x_1^*+L_2\right)^2+H^2\right)+\sigma^2}\right)}$. The UAV will associate with the last two devices and we now have $T_6 = T_{61} + T_{62}$.
  Another scheme is during the first interval $(0, T_7/2]$, UAV 1 associates with device 1 and collects data at $\left[-x_4^*, 0\right]$, and simultaneously, UAV 2 associates with device 3 and harvests at $[x_3^*, 0]$; and within the second interval $(T_7/2, T_7]$, UAV 1 associates with device 2 and collects data at $[-x_3^*, 0]$, and simultaneously, UAV 2 associates with device 4 and harvests at $\left[x_4^*, 0\right]$, where $T_7 = \frac{2D_u}{B\log_2\left(1+\frac{\beta_0 p_u/\left(\left(x_3^*-x_2\right)^2+H^2\right)}{\beta_0 p_u/\left(\left(x_3^*+x_1\right)^2+H^2\right)+\sigma^2}\right)}$. As the complicated expression of the rate, it is hard to give an insightful closed-form result, thus picking up the minimal completion of strategy leading to the optimal solution, thus we have $T_5^* = \min\{T_6, T_7\}$.

Finally, by combining the above five cases and Lemma 2, we have $T_1^* \geq T_2^* \geq T_3^* \geq T_4^* \geq T_5^*$ and the proposition is proved.

Appendix B. Proof of Proposition 2

First, we will give a lower bound of $\bar{R}_{n,u}[i]$ by exploiting the minimal interference distance as follows,

$$\begin{aligned}\bar{R}_{n,u}[i]\left(\tilde{\mathbf{q}}_n'^r[i], \tilde{\alpha}_{n,u}'^r[i]\right) &= \log_2\left(1+\frac{\frac{\beta_0 p_u}{\left(\check{L}_{n,i}^2+H^2\right)^{\alpha/2}}}{\sum_{k=1,k\neq n}^{N}\frac{\beta_0 p_u}{\left(\left\|\mathbf{w}_{\mathrm{X}_k[i]}-\tilde{\mathbf{q}}_n'^r[i]\right\|^2+H^2\right)^{\alpha/2}}+\sigma^2}\right)\\ &\geq \log_2\left(1+\frac{\frac{\beta_0 p_u}{\left(\check{L}_{n,i}^2+H^2\right)^{\alpha/2}}}{\left(\frac{(N-1)\times\beta_0 p_u}{\left(\hat{L}_{n,i}^2+H^2\right)^{\alpha/2}}+\sigma^2\right)}\right)\end{aligned} \tag{A5}$$

where $X_n[i] = \{u|\tilde{\alpha}'_{n,u}[i] = 1\}$, $\check{L}_{n,i} = \left\|\mathbf{w}_{X_n[i]} - \tilde{q}'^r_n[i]\right\|$ and $\hat{L}_{n,i} = \min_{k\in\mathcal{N},k\neq n}\left\|\mathbf{w}_{X_k[i]} - \tilde{q}'^r_n[i]\right\|$. Then, we assume that there are χ UAVs co-workiing in the same time, and plug the above expression (A5) into the following equation, and then we have,

$$\frac{1}{\chi}\log_2\left(1+\frac{\beta_0 p_u}{\left(\check{L}^2_{n,i}+H^2\right)^{\alpha/2}\sigma^2}\right) \simeq \log_2\left(1+\frac{\left(\hat{L}^2_{n,i}+H^2\right)^{\alpha/2}}{(\chi-1)\times\left(\check{L}^2_{n,i}+H^2\right)^{\alpha/2}}\right)$$
$$\Rightarrow \left(1+\frac{\beta_0 p_u}{\left(\check{L}^2_{n,i}+H^2\right)^{\alpha/2}\sigma^2}\right)^{1/\chi} - 1 = \frac{\left(\hat{L}^2_{n,i}+H^2\right)^{\alpha/2}}{(\chi-1)\times\left(\check{L}^2_{n,i}+H^2\right)^{\alpha/2}} \quad \text{(A6)}$$

Thus, when the right-hand side of the equation is larger, the rate of IC schemes outperforms the TD scheme, otherwise the performance of TD scheme is better. The proof is complete.

References

1. Motlagh, N.H.; Bagaa, M.; Taleb, T. UAV-based IoT platform: A crowd surveillance use case. *IEEE Commun. Mag.* **2017**, *55*, 128–134. [CrossRef]
2. Salmoral, G.; Rivas Casado, M.; Muthusamy, M.; Butler, D.; Menon, P.P.; Leinster, P. Guidelines for the Use of Unmanned Aerial Systems in Flood Emergency Response. *Water* **2020**, *12*, 521. [CrossRef]
3. Langhammer, J.; Lendzioch, T.; Miřijovský, J.; Hartvich, F. UAV-based optical granulometry as tool for detecting changes in structure of flood depositions. *Remote Sens.* **2017**, *9*, 240. [CrossRef]
4. Yang, Y.; Zheng, Z.; Bian, K.; Song, L.; Han, Z. Real-Time Profiling of Fine-Grained Air Quality Index Distribution Using UAV Sensing. *IEEE Internet Things J.* **2018**, *5*, 186–198. [CrossRef]
5. Ortiz, S.; Calafate, C.T.; Cano, J.C.; Manzoni, P.; Toh, C.K. A UAV-based content delivery architecture for rural areas and future smart cities. *IEEE Internet Comput.* **2018**, *23*, 29–36. [CrossRef]
6. Alsalam, B.H.Y.; Morton, K.; Campbell, D.; Gonzalez, F. Autonomous UAV with vision based on-board decision making for remote sensing and precision agriculture. In Proceedings of the 2017 IEEE Aerospace Conference, Big Sky, MT, USA, 4–11 March 2017; pp. 1–12.
7. Zeng, Y.; Zhang, R.; Lim, T.J. Wireless Communications with Unmanned Aerial Vehicles: Opportunities and Challenges. *IEEE Commun. Mag.* **2016**, *54*, 36–42. [CrossRef]
8. Hayat, S.; Yanmaz, E.; Muzaffar, R. Survey on Unmanned Aerial Vehicle Networks for Civil Applications: A Communications Viewpoint. *IEEE Commun. Surv. Tutor.* **2016**, *18*, 2624–2661. [CrossRef]
9. Mozaffari, M.; Saad, W.; Bennis, M.; Nam, Y.H.; Debbah, M. A Tutorial on UAVs for Wireless Networks: Applications, Challenges, and Open Problems. *IEEE Commun. Surv. Tutor.* **2019**, *21*, 2334–2360. [CrossRef]
10. Huo, Y.M.; Dong, X.D.; Lu, T.; Xu, W.; Yuen, M. Distributed and Multilayer UAV Networks for Next-Generation Wireless Communication and Power Transfer: A Feasibility Study. *IEEE Internet Things J.* **2019**, *6*, 7103–7115. [CrossRef]
11. Zeng, Y.; Wu, Q.; Zhang, R. Accessing from the sky: A tutorial on UAV communications for 5G and beyond. *Proc. IEEE* **2019**, *107*, 2327–2375. [CrossRef]
12. Li, B.; Fei, Z.S.; Zhang, Y. UAV Communications for 5G and Beyond: Recent Advances and Future Trends. *IEEE Internet Things J.* **2019**, *6*, 2241–2263. [CrossRef]
13. Mozaffari, M.; Saad, W.; Bennis, M.; Debbah, M. Mobile Internet of Things: Can UAVs provide an energy-efficient mobile architecture? In Proceedings of the 2016 IEEE Global Communications Conference (GLOBECOM), Washington, DC, USA, 4–8 December 2016; pp. 1–6.
14. Katikala, S. Google project loon. *InSight Rivier Acad. J.* **2014**, *10*, 1–6.
15. Takacs, A.; Lin, X.; Hayes, S.; Tejedor, E. Drones and networks: Ensuring Safe and Secure Operations. 2018. Available online: https://www.ericsson.com/en/reports-and-papers/white-papers/drones-and-networks-ensuring-safe-and-secure-operations (accessed on 22 December 2020).
16. Mitchell, G. Facebook's Internet-Delivering Drone Takes Flight. 2017. Available online: https://www.usatoday.com/story/tech/nation-now/2017/06/30/facebooks-internet-delivering-drone-takes-flight/444559001/ (accessedd on 22 December 2020).
17. EE Pioneers 'Air Mast' Technology for Rural Mobile Coverage and Disaster Recovery. 2020. Available online: https://newsroom.ee.co.uk/ee-pioneers-air-mast-technology-for-rural-mobile-coverage-and-disaster-recovery/ (accessed on 22 December 2020).
18. When COWs Fly: AT&T Sending LTE Signals From Drones. 2020. Available online: https://about.att.com/innovationblog/cows_fly (accessed on 22 December 2020).
19. Dhillon, H.S.; Huang, H.; Viswanathan, H. Wide-area wireless communication challenges for the Internet of Things. *IEEE Commun. Mag.* **2017**, *55*, 168–174. [CrossRef]

20. Zhan, C.; Zeng, Y.; Zhang, R. Energy-efficient data collection in UAV enabled wireless sensor network. *IEEE Wirel. Commun. Lett.* **2017**, *7*, 328–331. [CrossRef]
21. Mozaffari, M.; Saad, W.; Bennis, M.; Debbah, M. Mobile Unmanned Aerial Vehicles (UAVs) for Energy-Efficient Internet of Things Communications. *IEEE Trans. Wirel. Commun.* **2017**, *16*, 7574–7589. [CrossRef]
22. Gong, J.; Chang, T.H.; Shen, C.; Chen, X. Flight Time Minimization of UAV for Data Collection Over Wireless Sensor Networks. *IEEE J. Sel. Areas Commun.* **2018**, *36*, 1942–1954. [CrossRef]
23. Mozaffari, M.; Saad, W.; Bennis, M.; Debbah, M. Efficient deployment of multiple unmanned aerial vehicles for optimal wireless coverage. *IEEE Commun. Lett.* **2016**, *20*, 1647–1650. [CrossRef]
24. Alzenad, M.; El-Keyi, A.; Lagum, F.; Yanikomeroglu, H. 3-D Placement of an Unmanned Aerial Vehicle Base Station (UAV-BS) for Energy-Efficient Maximal Coverage. *IEEE Wirel. Commun. Lett.* **2017**, *6*, 434–437. [CrossRef]
25. Bor-Yaliniz, R.I.; El-Keyi, A.; Yanikomeroglu, H. Efficient 3-D placement of an aerial base station in next generation cellular networks. In Proceedings of the 2016 IEEE international conference on communications (ICC), Kuala Lumpur, Malaysia, 22–27 May 2016; pp. 1–5.
26. Alzenad, M.; El-Keyi, A.; Yanikomeroglu, H. 3-D Placement of an Unmanned Aerial Vehicle Base Station for Maximum Coverage of Users With Different QoS Requirements. *IEEE Wirel. Commun. Lett.* **2018**, *7*, 38–41. [CrossRef]
27. Azari, M.M.; Rosas, F.; Chen, K.C.; Pollin, S. Ultra Reliable UAV Communication Using Altitude and Cooperation Diversity. *IEEE Trans. Commun.* **2018**, *66*, 330–344. [CrossRef]
28. Azari, M.M.; Rosas, F.; Pollin, S. Cellular Connectivity for UAVs: Network Modeling, Performance Analysis, and Design Guidelines. *IEEE Trans. Wirel. Commun.* **2019**, *18*, 3366–3381. [CrossRef]
29. He, H.; Zhang, S.; Zeng, Y.; Zhang, R. Joint Altitude and Beamwidth Optimization for UAV-Enabled Multiuser Communications. *IEEE Commun. Lett.* **2018**, *22*, 344–347. [CrossRef]
30. Xue, Y.; Xu, B.; Xia, W.; Zhang, J.; Zhu, H. Backhaul-Aware Resource Allocation and Optimum Placement for UAV-Assisted Wireless Communication Network. *Electronics* **2020**, *9*, 1397. [CrossRef]
31. Lyu, J.; Zeng, Y.; Zhang, R.; Lim, T.J. Placement Optimization of UAV-Mounted Mobile Base Stations. *IEEE Commun. Lett.* **2017**, *21*, 604–607. [CrossRef]
32. Mozaffari, M.; Saad, W.; Bennis, M.; Debbah, M. Optimal Transport Theory for Cell Association in UAV-Enabled Cellular Networks. *IEEE Commun. Lett.* **2017**, *21*, 2053–2056. [CrossRef]
33. Koyuncu, E.; Shabanighazikelayeh, M.; Seferoglu, H. Deployment and Trajectory Optimization of UAVs: A Quantization Theory Approach. *IEEE Trans. Wirel. Commun.* **2018**, *17*, 8531–8546. [CrossRef]
34. Qiu, C.; Wei, Z.; Feng, Z.; Zhang, P. Joint Resource Allocation, Placement and User Association of Multiple UAV-Mounted Base Stations With In-Band Wireless Backhaul. *IEEE Wirel. Commun. Lett.* **2019**, *8*, 1575–1578. [CrossRef]
35. Mozaffari, M.; Saad, W.; Bennis, M.; Debbah, M. Drone small cells in the clouds: Design, deployment and performance analysis. In Proceedings of the 2015 IEEE Global Communications Conference (GLOBECOM), San Diego, CA, USA, 6–10 December 2015; pp. 1–6.
36. Wu, Q.; Xu, J.; Zhang, R. Capacity Characterization of UAV-Enabled Two-User Broadcast Channel. *IEEE J. Sel. Areas Commun.* **2018**, *36*, 1955–1971. [CrossRef]
37. Zhong, X.; Huo, Y.; Dong, X.; Liang, Z. QoS-Compliant 3-D Deployment Optimization Strategy for UAV Base Stations. *IEEE Syst. J.* **2020**, 1–9. [CrossRef]
38. Liu, L.; Zhang, S.W.; Zhang, R. CoMP in the Sky: UAV Placement and Movement Optimization for Multi-User Communications. *IEEE Trans. Commun.* **2019**, *67*, 5645–5658. [CrossRef]
39. Lyu, J.; Zeng, Y.; Zhang, R. Cyclical Multiple Access in UAV-Aided Communications: A Throughput-Delay Tradeoff. *IEEE Wirel. Commun. Lett.* **2016**, *5*, 600–603. [CrossRef]
40. Zeng, Y.; Zhang, R.; Lim, T.J. Throughput Maximization for UAV-Enabled Mobile Relaying Systems. *IEEE Trans. Commun.* **2016**, *64*, 4983–4996. [CrossRef]
41. Zhang, S.; Zhang, H.; He, Q.; Bian, K.; Song, L. Joint Trajectory and Power Optimization for UAV Relay Networks. *IEEE Commun. Lett.* **2018**, *22*, 161–164. [CrossRef]
42. Zhang, J.; Zeng, Y.; Zhang, R. UAV-Enabled Radio Access Network: Multi-Mode Communication and Trajectory Design. *IEEE Trans. Signal Process.* **2018**, *66*, 5269–5284. [CrossRef]
43. Mozaffari, M.; Saad, W.; Bennis, M.; Debbah, M. Unmanned aerial vehicle with underlaid device-to-device communications: Performance and tradeoffs. *IEEE Trans. Wirel. Commun.* **2016**, *15*, 3949–3963. [CrossRef]
44. Zeng, Y.; Zhang, R. Energy-Efficient UAV Communication With Trajectory Optimization. *IEEE Trans. Wirel. Commun.* **2017**, *16*, 3747–3760. [CrossRef]
45. Zeng, Y.; Xu, J.; Zhang, R. Energy Minimization for Wireless Communication With Rotary-Wing UAV. *IEEE Trans. Wirel. Commun.* **2019**, *18*, 2329–2345. [CrossRef]
46. Zhan, C.; Zeng, Y. Energy-Efficient Data Uploading for Cellular-Connected UAV Systems. *IEEE Trans. Wirel. Commun.* **2020**, *19*, 7279–7292. [CrossRef]
47. Yang, D.; Wu, Q.; Zeng, Y.; Zhang, R. Energy Tradeoff in Ground-to-UAV Communication via Trajectory Design. *IEEE Trans. Veh. Technol.* **2018**, *67*, 6721–6726. [CrossRef]

48. Sun, Y.; Xu, D.F.; Ng, D.W.K.; Dai, L.L.; Schober, R. Optimal 3D-Trajectory Design and Resource Allocation for Solar-Powered UAV Communication Systems. *IEEE Trans. Commun.* **2019**, *67*, 4281–4298. [CrossRef]
49. Jiang, F.; Swindlehurst, A.L. Optimization of UAV heading for the ground-to-air uplink. *IEEE J. Sel. Areas Commun.* **2012**, *30*, 993–1005. [CrossRef]
50. Zeng, Y.; Xu, X.L.; Zhang, R. Trajectory Design for Completion Time Minimization in UAV-Enabled Multicasting. *IEEE Trans. Wirel. Commun.* **2018**, *17*, 2233–2246. [CrossRef]
51. Huang, Y.; Mei, W.; Xu, J.; Qiu, L.; Zhang, R. Cognitive UAV Communication via Joint Maneuver and Power Control. *IEEE Trans. Commun.* **2019**, *67*, 7872–7888. [CrossRef]
52. Samir, M.; Sharafeddine, S.; Assi, C.M.; Nguyen, T.M.; Ghrayeb, A. UAV Trajectory Planning for Data Collection from Time-Constrained IoT Devices. *IEEE Trans. Wirel. Commun.* **2020**, *19*, 34–46. [CrossRef]
53. Zhang, J.; Zeng, Y.; Zhang, R. Multi-Antenna UAV Data Harvesting: Joint Trajectory and Communication Optimization. *J. Commun. Inf. Netw.* **2020**, *5*, 86–99.
54. Wang, Z.; Duan, L.; Zhang, R. Adaptive deployment for UAV-aided communication networks. *IEEE Trans. Wirel. Commun.* **2019**, *18*, 4531–4543. [CrossRef]
55. Zhan, C.; Zeng, Y. Completion Time Minimization for Multi-UAV-Enabled Data Collection. *IEEE Trans. Wirel. Commun.* **2019**, *18*, 4859–4872. [CrossRef]
56. Liu, X.; Liu, Y.; Chen, Y.; Hanzo, L. Trajectory design and power control for multi-UAV assisted wireless networks: A machine learning approach. *IEEE Trans. Veh. Technol.* **2019**, *68*, 7957–7969. [CrossRef]
57. Wu, Q.Q.; Zeng, Y.; Zhang, R. Joint Trajectory and Communication Design for Multi-UAV Enabled Wireless Networks. *IEEE Trans. Wirel. Commun.* **2018**, *17*, 2109–2121. [CrossRef]
58. Shen, C.; Chang, T.H.; Gong, J.; Zeng, Y.; Zhang, R. Multi-UAV Interference Coordination via Joint Trajectory and Power Control. *IEEE Trans. Signal Process.* **2020**, *68*, 843–858. [CrossRef]
59. Xie, L.; Xu, J.; Zeng, Y. Common Throughput Maximization for UAV-Enabled Interference Channel With Wireless Powered Communications. *IEEE Trans. Commun.* **2020**, *68*, 3197–3212. [CrossRef]
60. Wu, Q.Q.; Liu, L.; Zhang, R. Fundamental Trade-Offs in Communication and Trajectory Design for Uav-Enabled Wireless Network. *IEEE Wirel. Commun.* **2019**, *26*, 36–44. [CrossRef]
61. Abdelkrim, N.; Aouf, N.; Tsourdos, A.; White, B. Robust nonlinear filtering for INS/GPS UAV localization. In Proceedings of the 2008 16th Mediterranean Conference on Control and Automation, Corsica, France, 25–27 June 2008; pp. 695–702.
62. Zhao, T.; Luo, C.; Zhou, J.; Guo, D.; Chen, N.; Casaseca-de-la Higuera, P. DoA Prediction Based Beamforming with Low Training Overhead for Highly-Mobile UAV Communication with Cellular Networks. *Appl. Sci.* **2020**, *10*, 4420. [CrossRef]
63. Al-Hourani, A.; Kandeepan, S.; Lardner, S. Optimal LAP Altitude for Maximum Coverage. *IEEE Wirel. Commun. Lett.* **2014**, *3*, 569–572. [CrossRef]
64. Mengali, U. *Synchronization Techniques for Digital Receivers*; Springer Science & Business Media: Berlin/Heidelberg, Germany, 2013.
65. Selim, S.Z.; Ismail, M.A. K-means-type algorithms: A generalized convergence theorem and characterization of local optimality. *IEEE Trans. Pattern Anal. Mach. Intell.* **1984**, *PAMI-6*, 81–87. [CrossRef]
66. Faigl, J.; Váňa, P.; Saska, M.; Báča, T.; Spurný, V. On solution of the dubins touring problem. In Proceedings of the 2017 European Conference on Mobile Robots (ECMR), Paris, France, 6–8 September 2017; pp. 1–6.
67. Pěnička, R.; Faigl, J.; Váňa, P.; Saska, M. Dubins orienteering problem. *IEEE Robot. Autom. Lett.* **2017**, *2*, 1210–1217. [CrossRef]
68. Bektas, T. The multiple traveling salesman problem: An overview of formulations and solution procedures. *Omega* **2006**, *34*, 209–219. [CrossRef]
69. Grant, M.; Boyd, S. *CVX: Matlab Software for Disciplined Convex Programming, Version 2.1*; CVX: San Ramon, CA, USA, 2014.
70. Inspire 2 Series. 2020. Available online: https://www.dji.com/cn/inspire-2/specs (accessed on 22 December 2020).